University of South Carolina
Scholar Commons

Theses and Dissertations

Fall 2021

Development of a Converging-Channel Drop Tower For Sphere Symmetric Isolated Single Droplet Combustion

Nicholas Alexander DeMaio

Follow this and additional works at: https://scholarcommons.sc.edu/etd

 Part of the Aerospace Engineering Commons

Recommended Citation

DeMaio, N. A.(2021). *Development of a Converging-Channel Drop Tower For Sphere Symmetric Isolated Single Droplet Combustion.* (Master's thesis). Retrieved from https://scholarcommons.sc.edu/etd/6672

This Open Access Thesis is brought to you by Scholar Commons. It has been accepted for inclusion in Theses and Dissertations by an authorized administrator of Scholar Commons. For more information, please contact digres@mailbox.sc.edu.

DEVELOPMENT OF A CONVERGING-CHANNEL DROP TOWER FOR SPHERE SYMMETRIC ISOLATED SINGLE DROPLET COMBUSTION

By

Nicholas Alexander DeMaio

Bachelor of Science in Mechanical Engineering
University of South Carolina, 2019

Submitted in Partial Fulfillment of the Requirements

For the Degree of Master of Science in

Aerospace Engineering

College of Engineering and Computing

University of South Carolina

2021

Accepted by:

Sang Hee Won, Director of Thesis

Tanvir Farouk, Reader

Tracey L. Weldon, Interim Vice Provost and Dean of the Graduate School

© Copyright by Nicholas Alexander DeMaio, 2021
All Rights Reserved.

DEDICATION

I dedicate this work to my grandfathers; Helmut F. Geiger, Civil Engineer and Architect, and Robert J. DeMaio who served in the navy. May they both rest in peace.

ACKNOWLEDGEMENTS

I want to thank my advisor Dr. Sang Hee Won for funding this research, and those in our lab for their help and support.

ABSTRACT

The dawn of a new Space Age is upon us; Microgravity combustion of hydrocarbon fuels is a popular method of research and characterization. This allows for a one-dimensional analysis by suppressing the buoyancy forces produced by gravity and the large temperature differential between the flame boundary and the surrounding air. The current testing methods are expensive and require extensive preparation on the researchers behalf. There is a need to investigate an alternative method that is inexpensive, repeatable, and comparable to the other approaches that coincides with the literature.

A low-cost converging-channel drop tower was designed and fabricated for sphero-symmetric single droplet combustion of n-alkane fuels to be comparable to that in the literature. A piezoelectric actuated droplet generator was created to control droplet size as they fell through a coiled Nickel-Chromium resistance wire to implement combustion. A blower style fan was implemented to draw surrounding air through the converging-channel which causes said air to accelerate at the same rate as the droplet falls, counteracting the strong velocity field caused by the large temperature differential and the resultant density gradient.

With having the ability to simulate microgravity combustion for 0.46 seconds, and investigation into the preferential vaporization potential of binary fuel mixtures in a one-dimensional environment. Mole fractions of 75/25 for iso-cetane/n-alkanes were tested and analyzed using nuclear magnetic resonance spectroscopy. The n-alkanes used

were n-Hexane, n-Heptane, n-Octane, n-Decane, n-Dodecane for their increasing molecular weight and vapor pressures. Preferential vaporization was more apparent in the lighter alkane mixtures while less apparent as the molecular weight increas

TABLE OF CONTENTS

LIST OF TABLES

LIST OF FIGURES

LIST OF SYMBOLS

A	Area
a	Acceleration
d	Distance
d	Diameter
g	Gravitational Constant
K	Kelvin
kg	Kilogram
MJ	Megajoule
v	Kinematic Viscosity of Air
P	Perimeter
p	Pressure
Q	Volumetric Flow Rate
ρ	Density
T	Thickness
t	Time
v	Velocity
$\forall$	Volume
x	Half of the Width
z	Direction of Fluid Flow

LIST OF ABBREVIATIONS

CFM ..... Cubic Feet per Minute

ICMOS..... Intensified Complementary Metal Oxide Semiconductor

NASA.....National Aeronautics and Space Administration

NMR ..... Nuclear Magnetic Resonance

CHAPTER 1

MICROGRAVITY FACILITIES & ENERGY USAGE

Ever since the onset of the space race in the mid to late 20th century the world has had an increasing fascination with the extraterrestrial. The launch of the Sputnik 1 Satellite by the Soviet Union in 1957 marked the start of the space age that would bring a host of new technological and scientific discoveries [1]. The microgravity environment of Space is unlike anything felt here on Earth; This supplied a unique opportunity for experimentation.

Microgravity, or weightlessness, alters many observable phenomena within the physical and life sciences. Systems and processes affected by microgravity include surface wetting and interfacial tension, multiphase flow and heat transfer, multiphase system dynamics, solidification, and fire phenomena and combustion. Microgravity induces a vast array of changes in organisms ranging from bacteria to humans, including global alterations in gene expression and 3-D aggregation of cells into tissue-like architecture [2]. For the scope of this research, only microgravity combustion will be discussed henceforth. Figure 1.1 illustrates a comparison between flames in a non-gravitational environment versus one with gravity. This disparity in burning characteristics is due to the buoyancy forces or lack thereof in a microgravity environment. In this absence of gravity, the buoyancy is suppressed, and the analyses can be reduced to much simpler one-dimensional systems which significantly reduces calculation and are simpler and easier to understand. A typical flame is around eight

times hotter than the surrounding ambient air; this causes a large density gradient over a small distance. This resultant gradient induces a strong velocity field that causes the flame to lift and point upward. Instabilities in this flow field can result in the flame moving and flickering [2-3].

Today there are several ways to run experiments in microgravity. Currently one of the primary methods is experimentation in space like on the International Space Station (ISS), where the microgravity is caused by being in a constant state of free fall while orbiting the Earth, even though at an altitude between 200 and 250 miles the gravity would be about 90% that of being at the surface. On the ISS gravity can be as low as 10^{-6} g [4-5]. Unlike the other methods, research onboard the ISS can last any amount of time given the station is in a constant state of weightlessness, as well as the ability to intervene during experiments. However, this option is very expensive due to the cost of transportation via rocket and having to pay the astronauts to conduct the experiments. Then there is experimentation on airplanes flying parabolically where the micro comes from the aircraft using a series of different flight maneuvers to achieve around 10-2 g of gravity. Airbus A310 ZERO-G is the world's largest airplane for parabolic flights [5-6]. Typical flight duration with the Airbus A310 ZERO-G is about two and half hours, this allows for 30 parabolas to be flown per flight in sets of five with two minutes intervals between parabolas and with four to six minutes between sets of parabolas. Figure 1.2 illustrates how these parabolic maneuvers for the Airbus A310 ZERO-G achieve weightlessness. For these flights, the force of gravity acting on the experiments that are attached to the aircraft floor are in the order of 10^{-2} g, while the ones free floating in the cabin are typically 10^{-3} g [6].

There is also experimentation with drop towers. The National Aeronautics and Space Administration (NASA) has a 24 meter, 2.2 second drop tower at NASA-Glenn Research Center that was converted from a fuel distillation tower in the ’60s to study the effect of microgravity on physical phenomena such as combustion and fluid dynamics. It was converted during the space race era to facilitate research, since man had yet to go to space there needed to be a way to study microgravity and its effects on fluids. Since then, there are now several facilities around the world with drop towers possessing micro gravity capability. NASA-Glenn in Ohio, ZARM in Germany, JAMIC and MGLAB in Japan to name a few. Currently, these towers only last a few seconds but can be repeated many times throughout the day. They can reach an acceleration of around 10^{-3}-10^{-4} g by having a capsule fall in free fall down the tower [7-11]. These towers primarily run combustion experiments due to the short time in free fall and the fast nature of flame propagation.

These methods are used to study the effect of fuel combustion in microgravity as to gain a better understanding of ignition, soot formation, flame propagation and flame extinction during combustion in low gravity as well as to better understand and characterize fuels, improve the efficiency of internal combustion engines and to evaluate potential fire hazards aboard spacecraft. Combustion research will lead to more efficient fuels, better fire safety, and a cleaner environment in a fossil fuel dominant world [12].

Fossil fuels have been the dominant source of energy production for over 100 years in the U.S. and other major countries [14]. Fuels such as coal, natural gas, petroleum and its derivatives were formed over millions of years from the anaerobic decomposition of plants and animals in the Earth’s crust. These solids, liquids, and gases

contain hydrocarbon chains which are the primary factor in the combustion process. Figure 1.3 displays the U.S. consumption of commodities for energy production since 1776. With an energy density of about 24 MJ/kg for coal and 16MJ/kg for wood, coal was a major foundation for American industrialization in the nineteenth century, it was cheap and a more efficient source of power for steam engines, furnaces, and forges across the United States [15-16].

With this rapid industrialization came a surge in technology, from more advanced motor cars and airplanes to instruments of war such as battleships and tanks. These innovations required an alternative source of energy. Black gold fueled the war effort on both sides in World War I and World War II causing huge demand for petroleum. Petroleum usage in the U.S. expanded nearly ten times from 1900 to 1950. Research increased the number of products made from oil and natural gas, including explosives, plastics, and artificial rubbers [14,17]. Since then, oil and its derivatives have been a huge contender in industry, and the research needed to improve efficiencies, reduce emissions, and create a better understanding of the fuels we use. With such an increase in industrialization and the use of hydrocarbon fuels, researchers started to draw concern towards emissions and the impacts they had on public health and the environment. In 1970 Congress passed the Clean Air Act and established the Environmental Protection Agency to regulate pollution amongst transportation vehicles. Compared to vehicles of the 1970s, cars and trucks today are roughly 99% cleaner due to the elimination of lead, desulfurization, and improved fuel chemistry thanks to combustion research sparked by emission regulations [18].

After Multiple oil crises in the U.S. and around the world, an increase in energy demand, and stricter regulations, governments pushed for alternate sources of clean energy to supply the people with. The use of natural gas has slowly been on the rise thanks in part to its higher energy density and lower CO_2 emissions. However, fracking to obtain natural gas has brought up many of its own ethical and environmental concerns [14,16-17]. Renewable resources such as wind, solar, hydroelectric, makeup only 12% of the U.S. energy production in 2020, seen in figure 1.4, but have been on the rise and will continue to increase and surpass coal and natural gas to be almost equal with petroleum by 2050 as seen in figure 1.5 [14,17]. This is thanks to cheaper technology, the automotive industries switch to produce electric vehicles, and incentives from the government for people to have electric vehicles and use solar panels. Furthermore, the countries representing more than 65% of harmful greenhouse gasses and more than 70% of the world economy will have committed to achieving net zero emissions by 2050.

Fossil fuels have been for the last 100 years, are, and will continue to be the dominant source of energy production in most major countries and for the next 100 years. For the scope of humanity, it is a short-term solution for the long-term problem that is the ever evolving technology that continues to demand more and more energy.

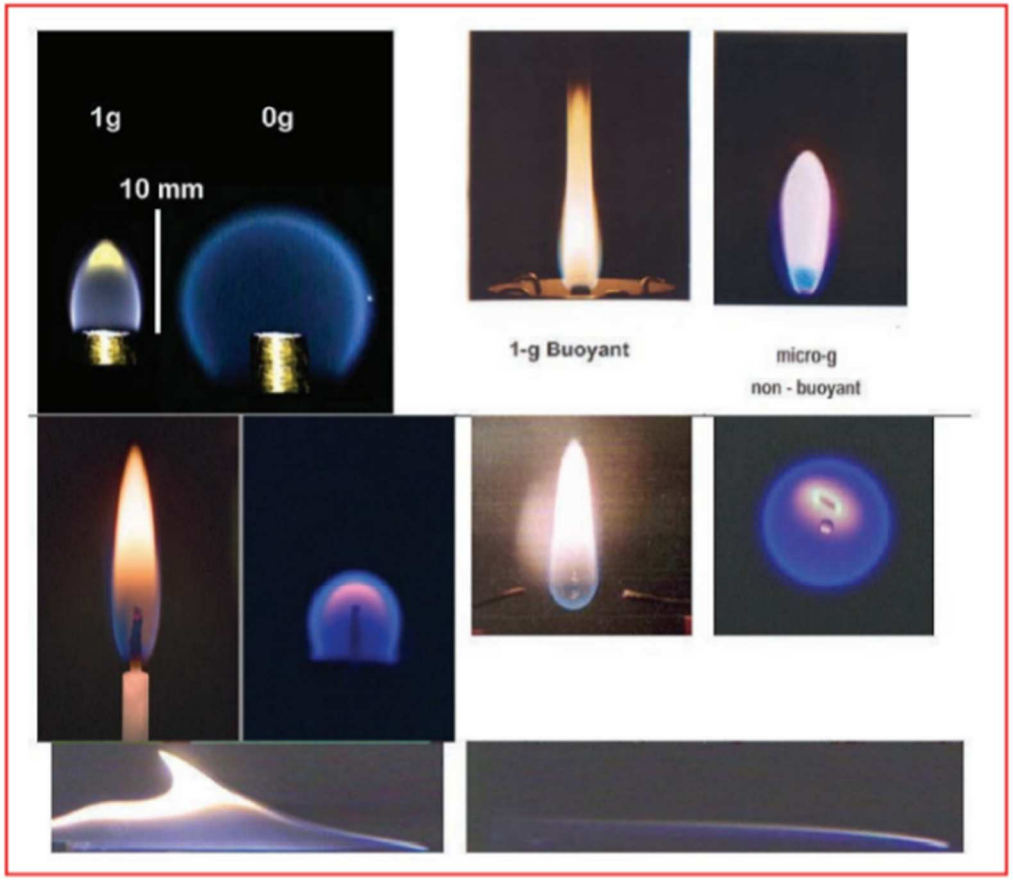

Figure 1.1: Comparison of Flames in Microgravity and Non-Microgravity

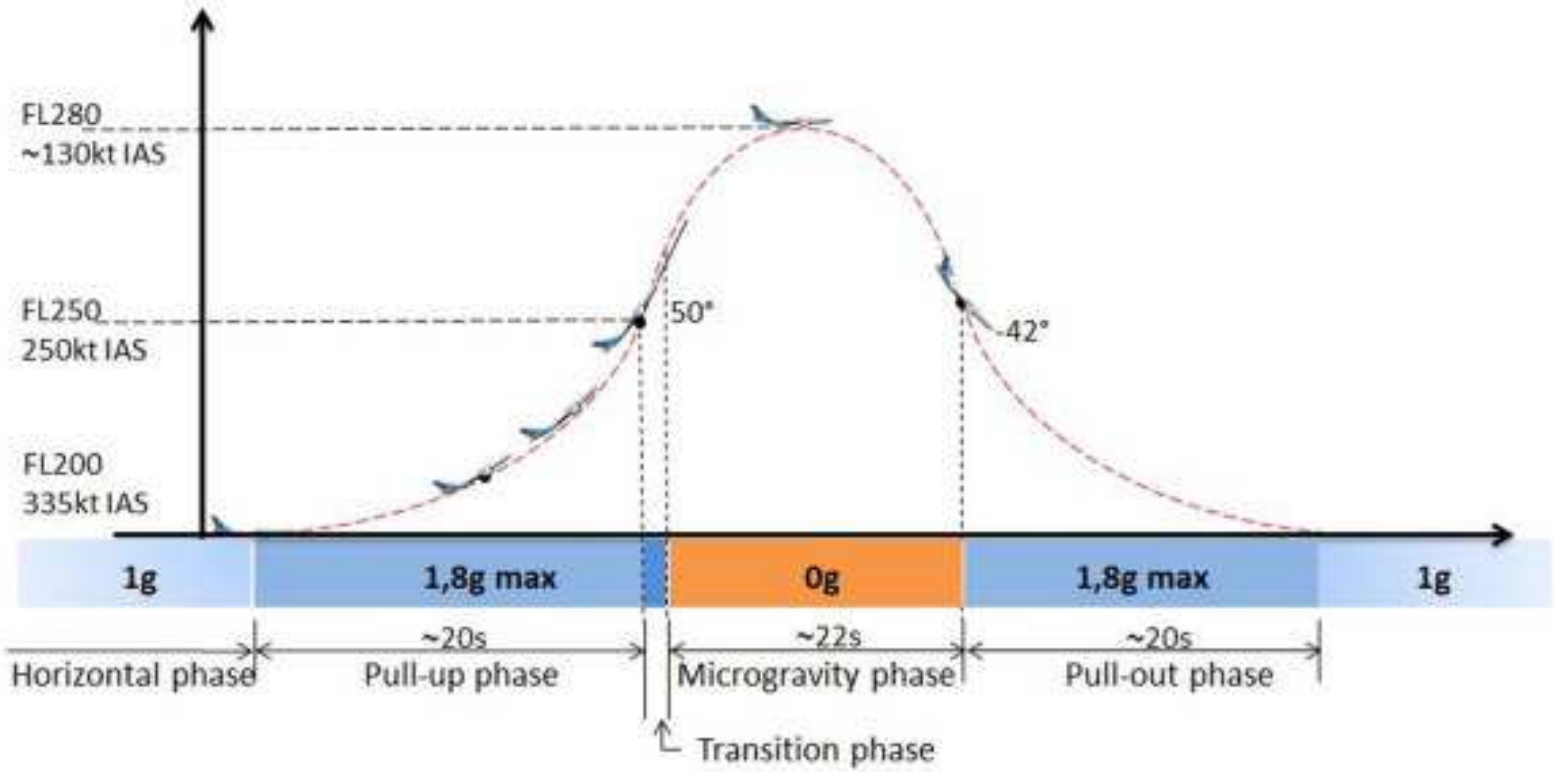

Figure 1.2: Flight Path of an Airbus A310 During Microgravity Experimentation

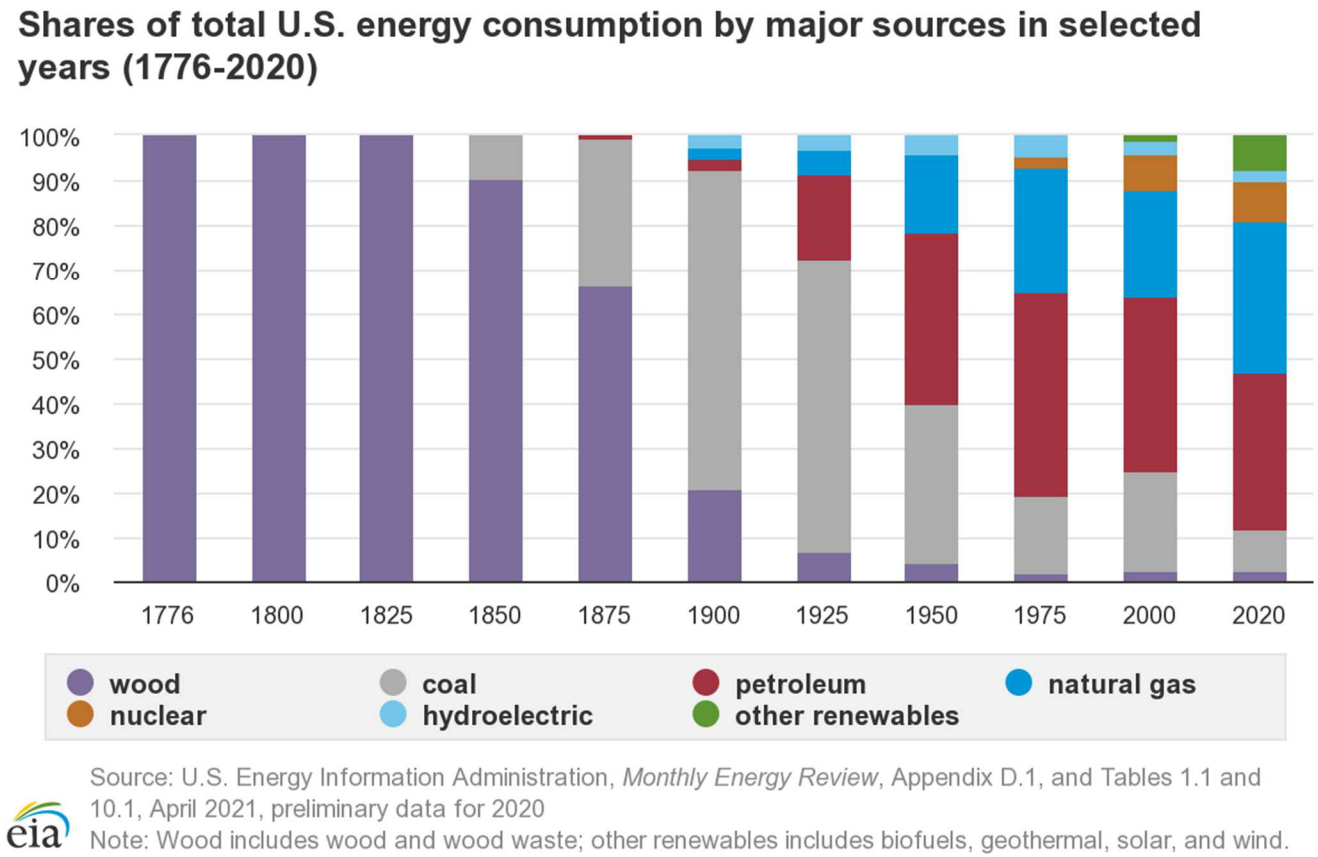

Figure 1.3: The Production Source of Energy in the U.S. From 1776 Through 2020.

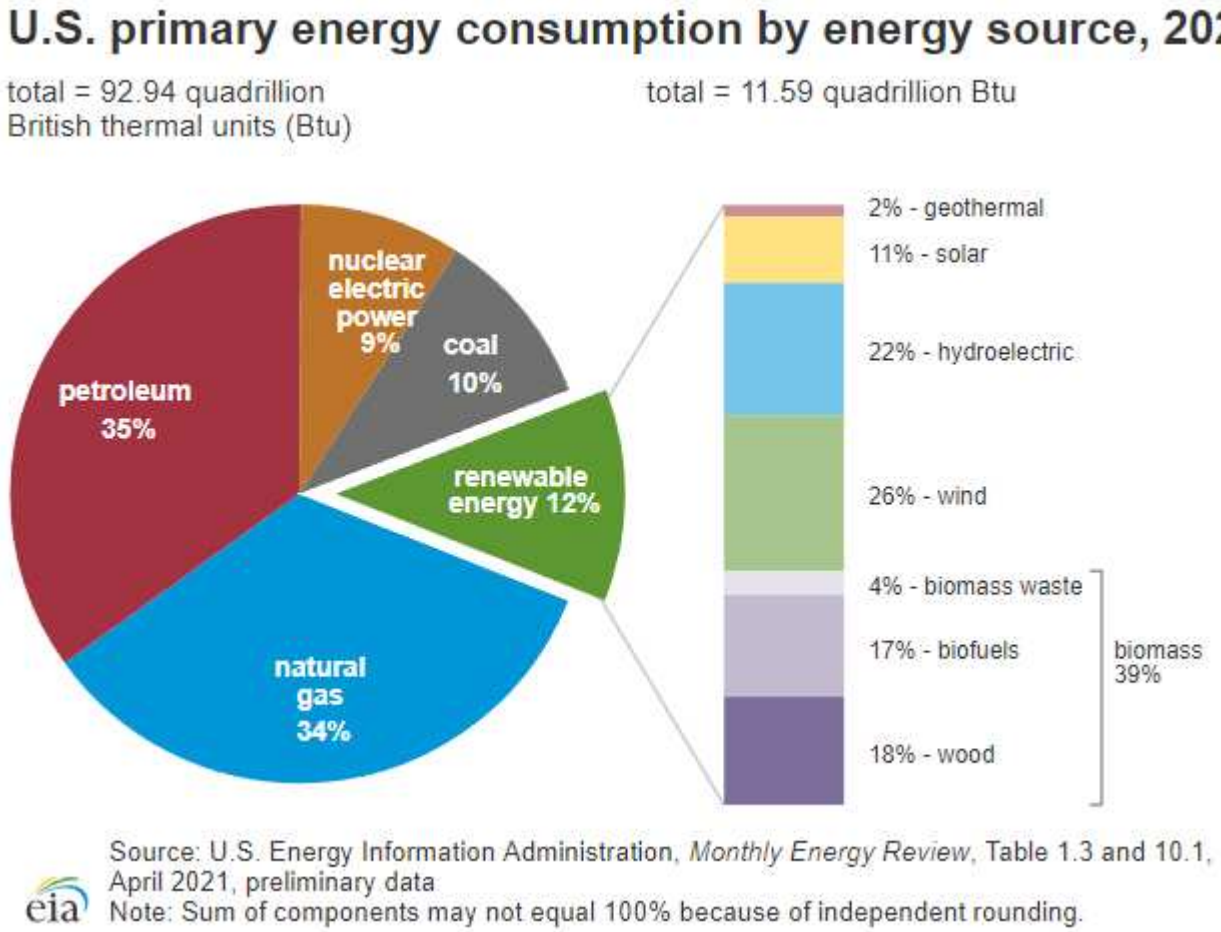

Figure 1.4: Energy Consumption by Source in 2020

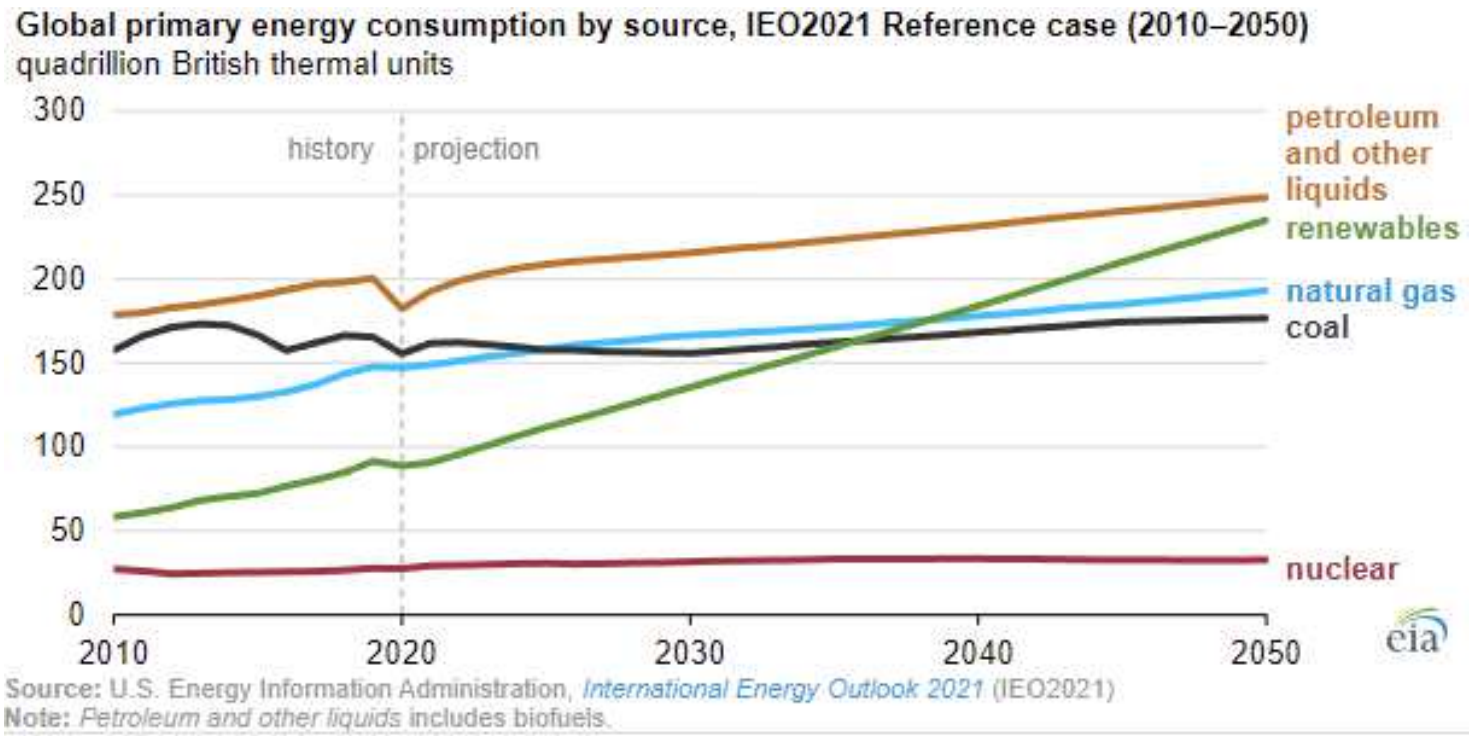

Figure 1.5: Energy Consumption Prediction or the Next 30 Years

CHAPTER 2

PREVIOUS MICROGRAVITY EXPERIMENTATION

Despite being the subject of active research for over 80 years, combustion processes remain one of the most poorly controlled phenomena that have a significant impact on human health, comfort, and safety [2]. Combustion on a layman scale consists of two things, fuel and air. This generates carbon dioxide, water, and releases energy in the form of heat. Below is the basic stoichiometry for the combustion of methane,

$$CH_4 + 2O_2 \rightarrow CO_2 + 2H_2O \qquad (2.1)$$

Fuel, methane, plus air, oxygen, generates CO_2 and H_2O; That is Combustion. Even the simplest forms of combustion remain beyond our detailed numerical modeling capabilities, typical combustion processes can involve hundreds of chemical species and thousands of reactions. The species and reactions determine chemical kinetics, flammability limits and pollutant emissions of fuels. Small scale experiments can be performed, however, buoyant forces due to gravity tend to dominate which obscures and complicates analysis. In the presence of microgravity, buoyancy created from the large temperature differential and subsequent density gradient between the flame and air is suppressed which leads to a much simpler one-dimensional analysis to align with the study and modeling of flame behavior.

Using the methods discussed in length in the previous chapter, researchers can recreate microgravity here on earth and extract fundamental data to better understand

combustion phenomena, as well as to study fire suppression techniques to minimize risk on spacecraft. Research conducted on the International Space Station includes topics such as the Flame Extinguishment Experiment in the paper by V. Nayagam et. al, where the objective is to study heptane and methanol droplets in ambient mixtures of oxygen and nitrogen mixed with other inert gasses, with the goal to examine how the addition of an inert gas suppressant influences the flammability limit of the two fuels. The physical and chemical kinetic models of heptane and methanol combustion are the basis for more complex models like diesel and jet fuel. These experiments performed demonstrated radiative and diffusive extinction, combustion instabilities, lower flammability limits, and recently discovered cool flame. [2,20]. Then there is the Structure & Liftoff In Combustion Experiment, which investigates the structure of lifting and lifted flames where flow conditions and the combustion chemistry cause the flame to detach from the burner and stabilize at a downstream position. This research helps to increase fuel efficiency and reduce pollutant emission in practical combustion devices by improving combustion modeling capabilities [2,21].

Previous experimentation in microgravity has not had the opportunity to collect droplets mid combustion, with the creation of the drop tower described in this paper, that becomes possible. Air is accelerated through the converging tube to match the droplet velocity at each location. As the droplet is in free fall, the surrounding air has negligible relative motion to the droplet. This effect is similar to how microgravity drop towers operate, the droplet and air inside the capsule are both in free fall. However, here the drops were collected at the bottom and analyzed.

Work done by Farouk et al investigates preferential vaporization in microgravity at varying pressures of multi-component jet fuel surrogates using a numerical model. Three surrogate fuels were created to exhibit essentially identical pre-vaporized gas-phase combustion property targets. This model was compared against experimental data from Yu Cheng Liu et al, who used a 1.2 second drop tower [22]. The goal of the research in this paper is to not only have the ability to recreate similar data to that in microgravity experiments but also expand on them with further testing with the ability to collect the droplets.

There have been similar attempts at simulating microgravity through a small scale forced convection drop tower done by Wang et al [23] and Mun Young Choi [24]. In the paper by Wang et al, researchers conducted numerical simulation for a forced convection drop tower that used a variation of the free-injected droplet method which allowed significant reductions in forced and buoyant convection effects. Their model was used to construct a converging drop tube system that used a flat-flame burner to create hot-gas flow at the inlet, achieving an environment of over 1000 K. because of this there was significant heat loss, as high as 10-15 K/cm in the axial direction, which could cause fluctuations in fluid dynamics that were not present in the model that assumed constant fluid properties. A piezoelectric droplet generator was used to make droplets from 50 pm to about 300 pm, which would auto ignite in the hot exhaust gasses. here, the primary focus was on the study of flame ignition and extinction. [23]. Then in the paper by Mun Young Choi, more simulation was done to substantiate the concept of a forced convection drop tower using FLUENT fluid flow software. Choi theorized using a hot wire set up to

auto ignite the fuel as opposed to the flat-flame burner to prevent problems with heat transfer and fluid fluctuations [24].

The current testing methods for microgravity experimentation are expensive and require extensive preparation on the researchers behalf. There is a need to investigate an alternative method that is inexpensive, repeatable, and comparable to the other approaches that coincides with the literature while expanding on the capabilities and branching out to new testing possibilities.

CHAPTER 3

DESIGN & FABRICATION

A 1.5 meter tall tower using forced convection, Figure 3.6, similar to the work done in Wang et al [23] and Mun Young Choi [24], was designed and fabricated according to a specific geometry for one-dimensional isolated single droplet combustion. This caused the air being forced through it to accelerate at the same rate that a droplet fell. For a steady state, one-dimensional, incompressible, and inviscid flow of a fluid down a contoured tube, the air follows this partial differential equation,

$$\frac{dp}{dz} + pv\left(\frac{dv}{dz}\right) - \rho g = 0 \qquad (3.1)$$

The tube was designed to be contoured so that the flow accelerates which would lead to $\frac{dp}{dz} = 0$. With no pressure gradient, the bouncy forces are eliminated. This coupled with the equations of motion and flowrate below, the geometry, velocity, residence time, and Reynolds number were calculated based on a set of initial conditions seen in Table 3.1.

$$v = v_0 + at \qquad (3.2)$$

$$d = v_0 t + \frac{1}{2}at^2 \qquad (3.3)$$

$$t = \frac{-v_0 + \sqrt{v_0^2 + 2ad}}{a} \qquad (3.4)$$

$$Q = vA = \text{const.} \qquad (3.5)$$

$$x = \frac{Q}{2Tv} \qquad (3.6)$$

Table 3.1: Initial Conditions for Tower Calculations

Thickness [cm]	2.54
Width [cm]	10.16
Initial Velocity [cm/s]	20
Flow Rate [L/min]	154.84

The opening cross-sectional area of the tower is seen in figure 3.1. Equation *3*.3 was manipulated to solve for residence time and create equation *3*.4. The graph is seen in figure 3.2 is the amount of time that the droplet spends combusting in the tower. Then the time was used in equation *3*.2 to calculate the velocity profile in figure 3.3 which started with an initial velocity of .1 m/s. Having the initial design area of 1 in. by 4 in., and an initial velocity of .1 m/s, the flowrate was able to be calculated using equation *3*.5. From the mass conservation principle, the mass flow rate and the volume flow rate must be constant throughout the tower, which equation 6 uses to calculate half of the width for the cross-section area of the tower. Calculating the negative of equation *3*.6 gave the other half of the width seen in figure 3.4. Lastly, the Reynolds number was calculated with equation *3*.7 below and is seen in figure 3.5.

$$Re = \frac{vD_h}{\nu} \tag{3.7}$$

$$D_h = \frac{4(A)}{P} \tag{3.8}$$

Finding a balance between the geometry in figure 3.4 and the Reynolds number in figure 3.5 was critical. If the Reynolds number was too high, then the airflow would be turbulent through the tower. Lowering the initial velocity helped to reduce the Reynolds but caused the geometry to converge faster and decrease the exit width. Both aspects would create challenges in fabrication and testing, so the initial conditions in table 3.1 were chosen to be the best fit.

A 3D model of the geometry was created using the data in figure 3.4, then was given to the University of South Carolina machine shop to fabricate the contour out of 6061 aluminum. Two acrylic windows were also designed with an O-Ring cord grove to seal in the tower and prevent any loss in flowrate with twenty-four bolts holding them together. A 4 in., 195 CFM inline duct ventilation fan was attached to the bottom of the tower to draw air through and was connected to an autotransformer that controlled the flow rate by varying the voltage. The final design is seen in figure 3.6. There was a ceramic honeycomb structure at the inlet of the tower to promote uniform flow as air entered. A droplet generator was also designed, figure 3.7, and machined out of aluminum, acrylic, and a piezoelectric actuator to create and control droplet size out of varying size needle tips. Drops of sizes from .9 mm to 2.35 mm were used to test the limits of the drop tower, larger flames would interact with the boundary layer near the walls while small droplets would fully combust before reaching the bottom. A Harvard Apparatus PHD 2000 syringe pump was used to control fuel flow rate, while a function generator and amplifier were used to power the piezoelectric actuation that controlled droplet size. The droplets passed through a Nickel-Chromium alloy heating wire coil right below the droplet generator tip where they auto-ignited right as they started to descend. The heating wire started melting the acrylic walls after prolonged use so copper foil tape was used in the first 5 cm of the tower to aid in heat transfer and prevent future melting.

A Photron Fastcam SA-Z highspeed camera and an Andor iStar intensified complementary metal oxide semiconductor (ICMOS) camera were used to observe flame behavior and acquire images of the droplets and flames at different sections as they fell

down the tower. Schlieren imaging and Shadowgraph were utilized with the highspeed camera which showed density gradients in the air surrounding the droplet, which created great contrast between the bounds of the droplets and the background. This allowed the measuring of the change in droplet diameter down the tower. Both methods require a light source to reflect off a concave mirror to collimate the light, and the culminated light shines through the windows of the tower to another concave mirror on the other side which was reflected to the high-speed camera. For Schlieren imaging, a knife-edge is placed between the camera and mirror to cut off refracting light, which allowed the density gradients to be seen. The ICMOS took direct photographs of the droplets and was synced with the droplet generator through the function generator. This allowed for the capture of flame geometry and to verify the droplets are spherical along with measuring flame diameter.

After verifying the droplets were sphere symmetric, fuels were tested for preferential vaporization by collecting droplets for NMR. Binary fuel mixtures of 75/25 by mole fraction were prepared using 75% 2,2,4,4,6,8,8-heptamethylnonane (iso-Cetane), and 25% of n-Heptane, n-Octane, n-Decane, and n-Dodecane, totaling four binary mixtures. Fuel vaporization is strongly governed by fuel boiling characteristics which are dependent on molecular weight [25-27].

Table 3.2: Characteristics For Fuel Used

Fuel	Molar Mass (g/mol)	Boiling point (°C)
n-Heptane	100.21	98
n-Octane	114.23	126
n-Decane	142.29	174
n-Dodecane	170.33	216
Iso-Cetane	226.448	240

Table 3.2 shows the molecular weight and boiling point of the fuels used. Iso-Cetane was chosen to be 75% for its high boiling point, with the other n-alkanes being lower weight to see how preferential vaporization is affected in 1D. Table 3.3 shows the measured mole fractions of the mixtures for ~2.35 mm droplets, and table 3.4 is for ~.9 mm droplets A glass cup surrounded by dry ice was placed right below the outlet of the tower to collect the drops which were then prepared for NMR. Dry ice was used to keep the samples cool, which would prevent further evaporation as well as to extinguish the droplet flame and prevent the samples from catching fire. Depending on the droplet size, 50-100 droplets were needed for enough volume to analyze with NMR. The acquisition time for quantitative 1H spectra was 3 seconds with a 30-second relaxation delay. For the 13C spectra, Chromium (III) acetylacetonate ($CR(acac)_3$) was added as a relaxation agent to reduce the relaxation delay time to 40 seconds with a 3 second acquisition time. The ($CR(acac)_3$) was added until it reached 0.05 molarity in the sample. The solvent for this method was deuterated Chloroform, Chloroform-D, or $CDCl_3$ and is referenced at 77.20 ppm for the 13C spectrum and 7.26 ppm for the 1H spectrum. Proton NMR was primarily used for analyzing the change in functional groups from before and after combustion. The functional group peaks were analyzed, and through post processing the mole fraction through NMR was found.

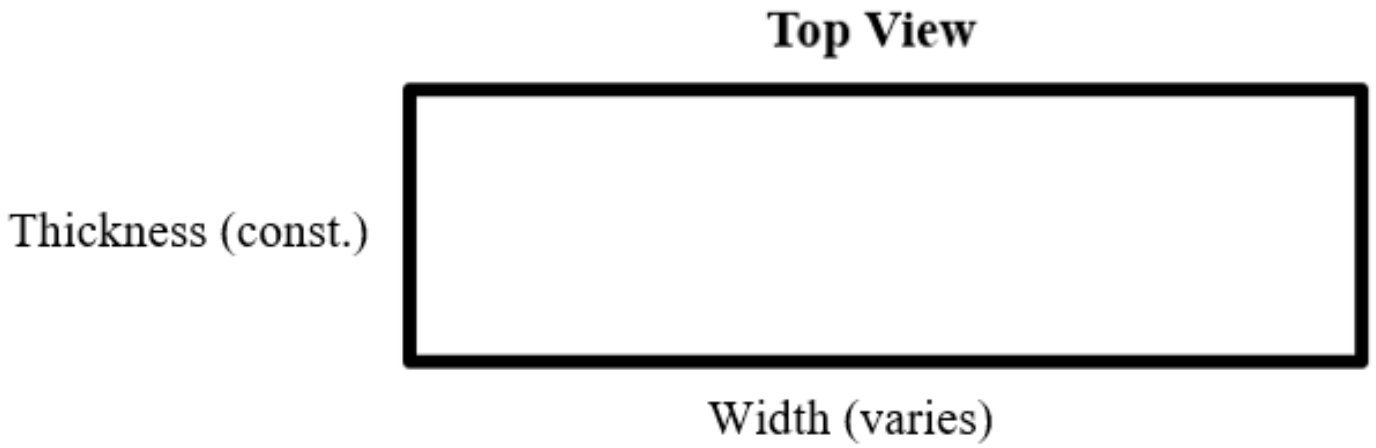

Figure 3.1: Cross-section Area of the Drop Tower

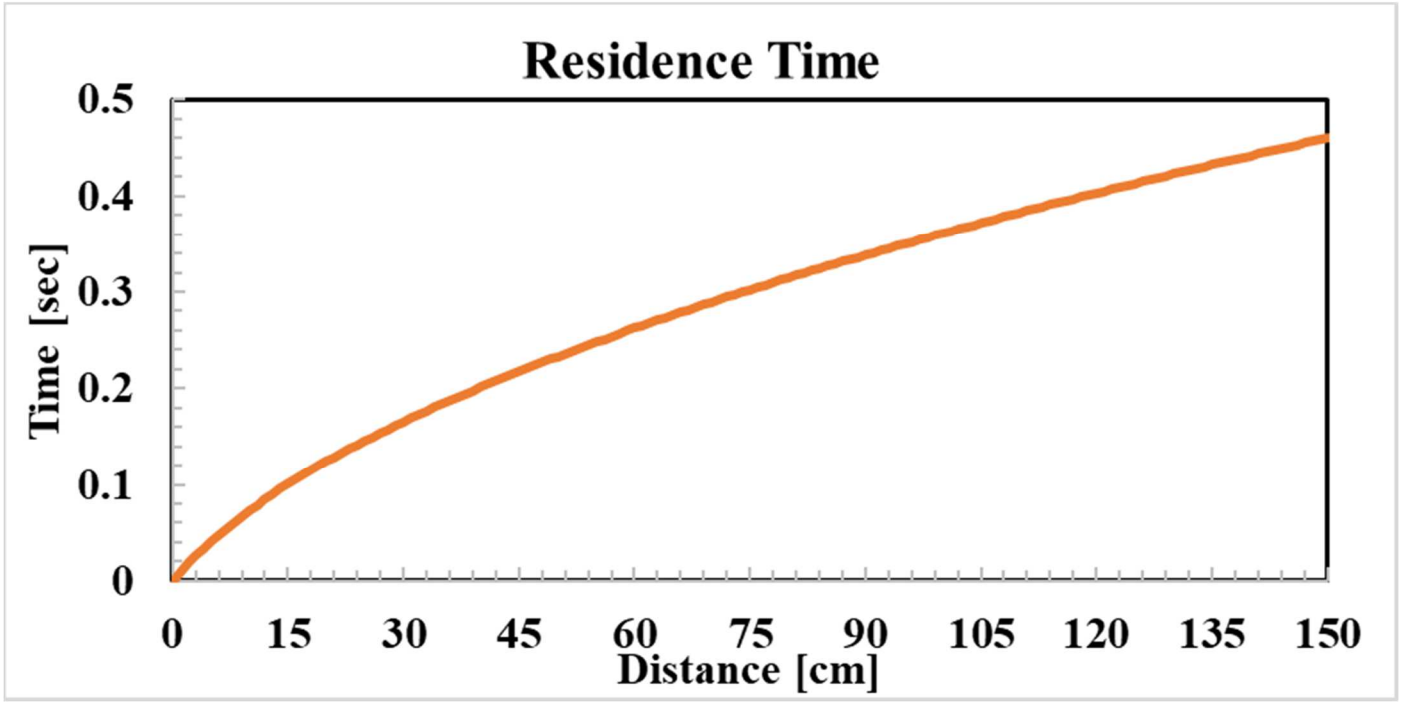

Figure 3.2: Residence Time for a Droplet in the Tower

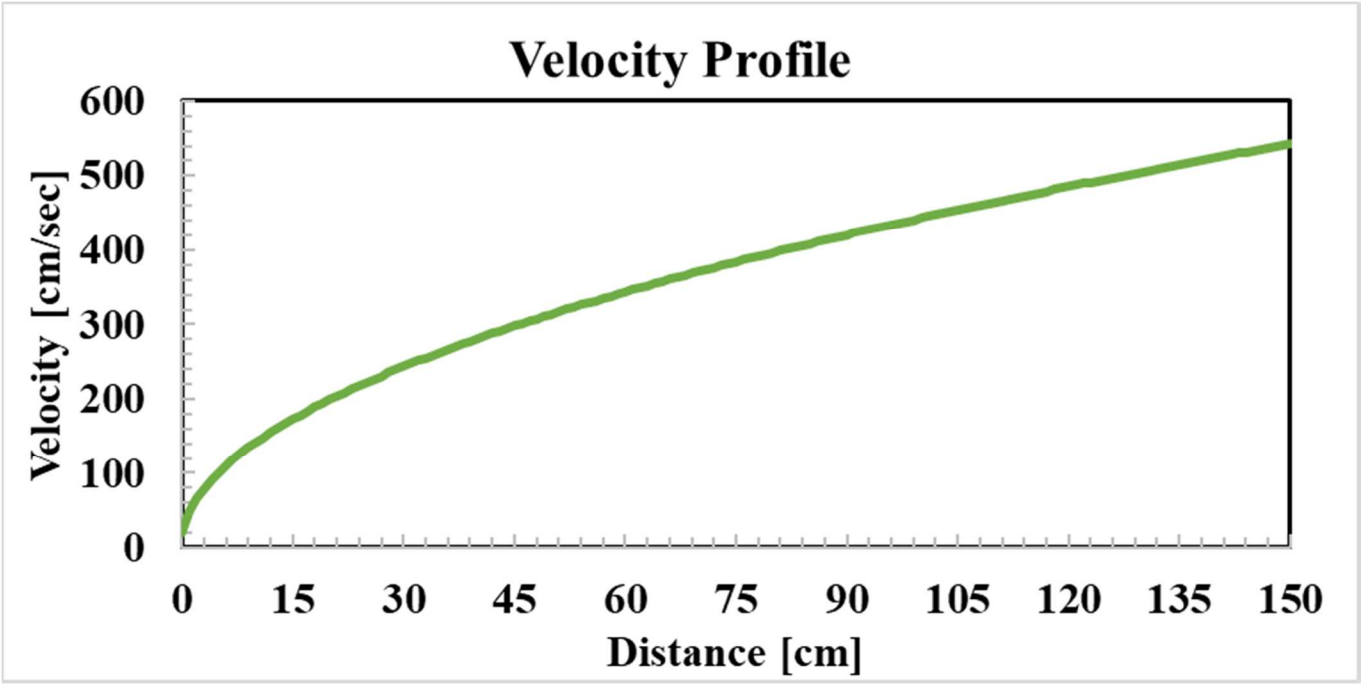

Figure 3.3: Velocity of a Droplet in the Tower

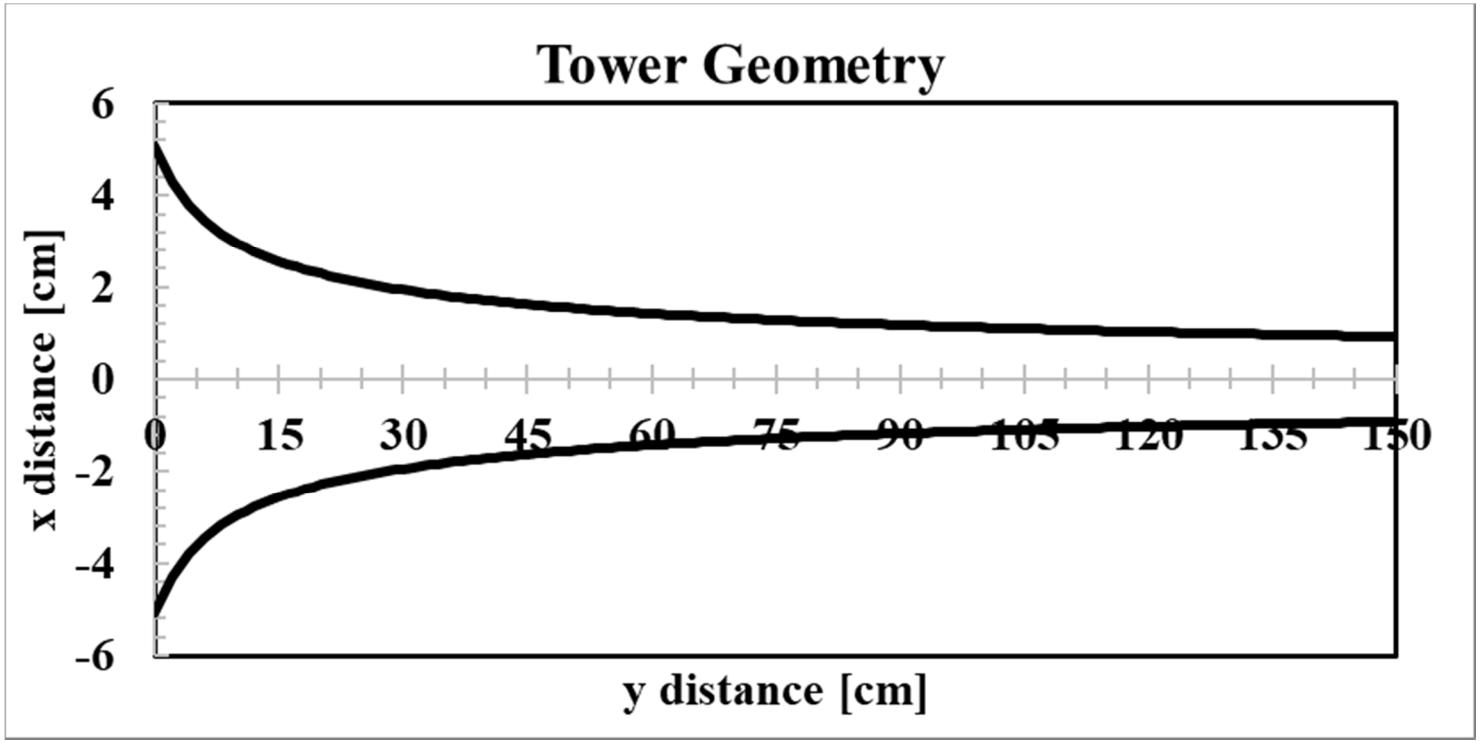

Figure 3.4: Shape of the Drop Tower

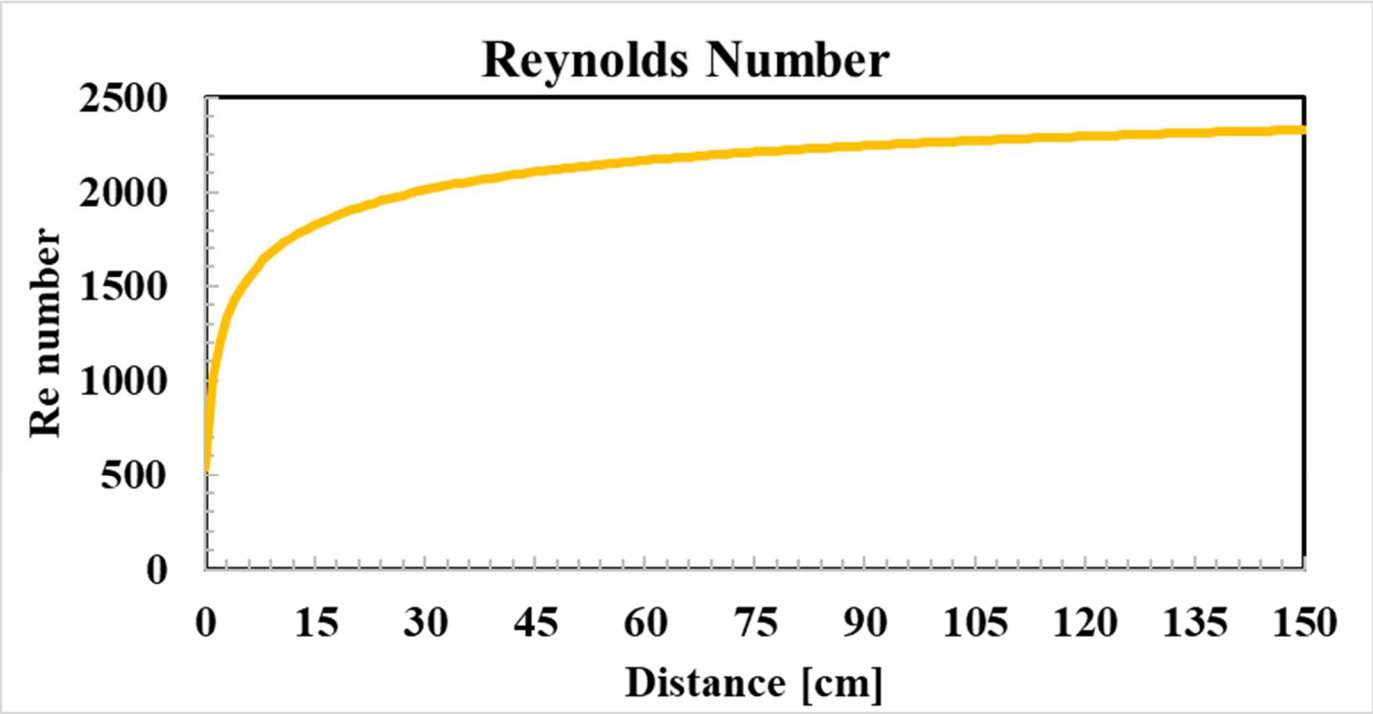

Figure 3.5: Reynolds Number Distribution

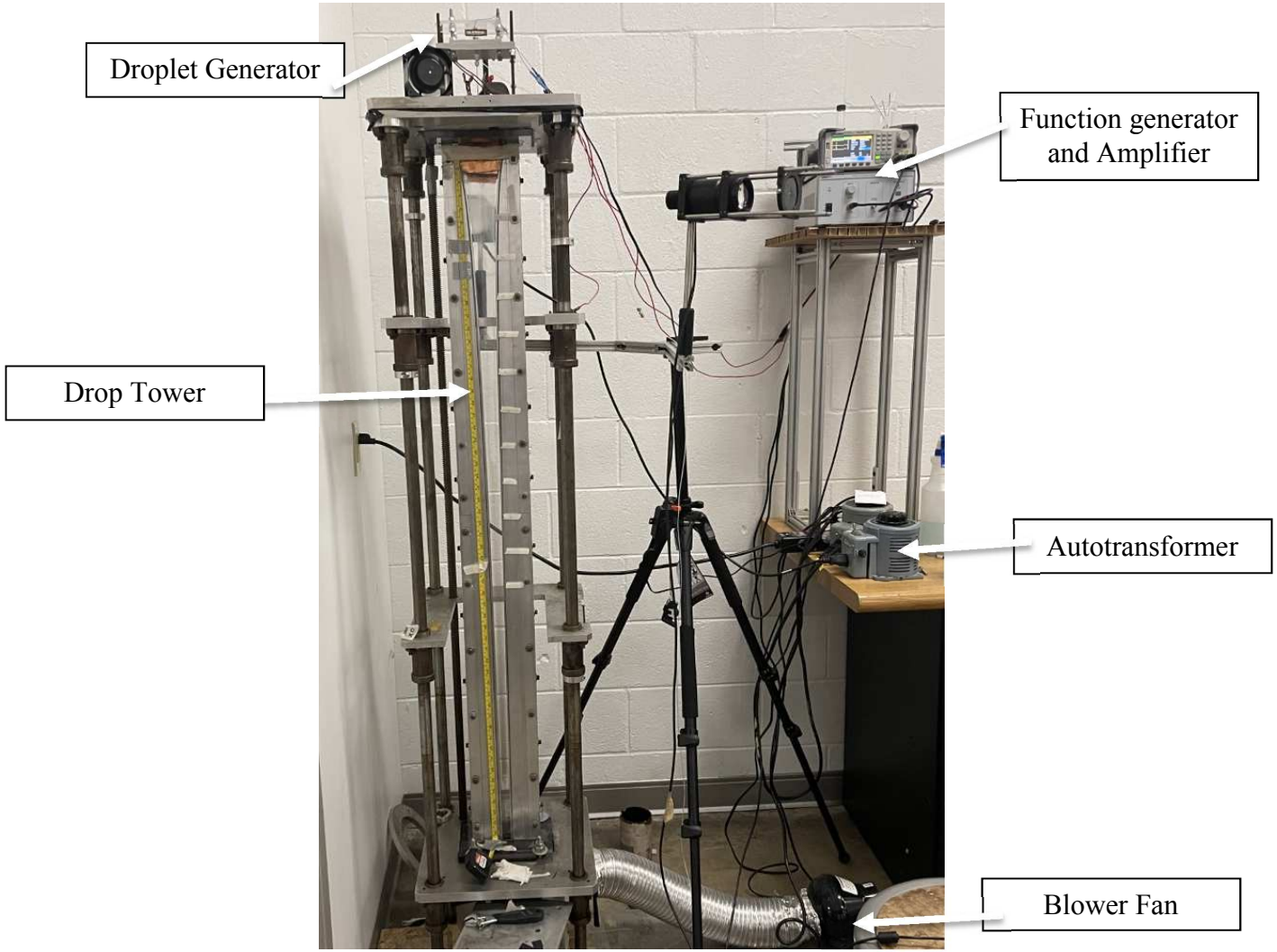

Figure 3.6: Drop Tower Setup

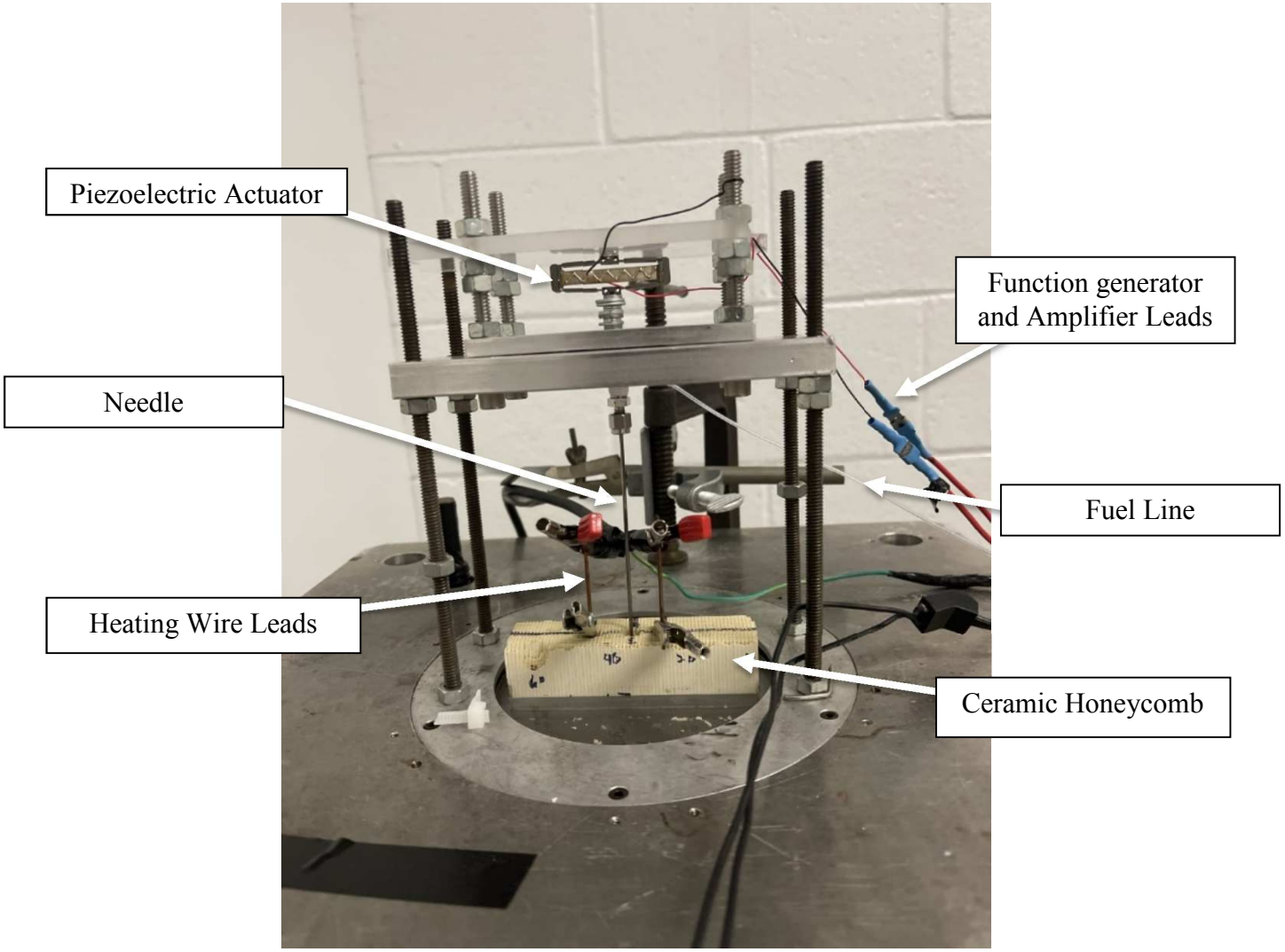

Figure 3.7: Droplet generator setup

Table 3.3: Measured Mole Fractions of n-Alkane Mixtures for ~2.35 mm Droplets

Mixture	Fuel	Measured Mass (g)	Measured Moles	Mole fraction (%)
Mixture 1	Iso-Cetane	16.9845	0.100114938	74.91786569
	n-Heptane	2.52675		25.18560174
Mixture 2	Iso-Cetane	16.9847	0.100067291	74.95442041
	n-Octane	2.868		25.09035635
Mixture 3	Iso-Cetane	15.2936	0.090283508	74.80537619
	n-Decane	3.2514		25.30973486
Mixture 4	Iso-Cetane	18.7547	0.110485669	74.96105394
	n-Dodecane	4.7145		25.05177748

Table 3.4: Measured Mole Fractions of n-Alkane Mixtures for ~.9 mm Droplets

Mixture	Fuel	Measured Mass (g)	Measured Moles	Mole fraction (%)
Mixture 1	Iso-Cetane	33.9795	0.100114938	74.91786569
	n-Heptane	5.02		25.18560174
Mixture 2	Iso-Cetane	16.9847	0.100067291	74.95442041
	n-Octane	2.868		25.09035635
Mixture 3	Iso-Cetane	32.275	0.090283508	74.80537619
	n-Decane	6.7944		25.30973486
Mixture 4	Iso-Cetane	31.43	0.110485669	74.96105394
	n-Dodecane	7.941		25.05177748

CHAPTER 4

RESULTS & DISCUSSION

The first droplet size tested was around 2.35 mm using n-Heptane. These were created with a slight pulse from the piezoelectric actuator right before gravity overcame the surface tension of the fuel on the needle. The flow rate of the blower was varied until the droplets were spherical, then images were taken down the height of the tower using the ICMOS camera to view the flame geometry. It was found was that as the droplet fell down the tower, they would stretch at both ends as the cross-sectional area became smaller and smaller.

Figure 4.1 shows the change in flame geometry as the drops traveled down the tower. It was concluded that the boundary layer along the walls of the tower was interacting with the flame front which caused it to stretch. The solution to this was to create smaller droplets that would have smaller diameter flames that would not interact with the boundary layer. By changing variables on the function generator connected to the piezoelectric actuator on the droplet generator, the droplet diameters were made to be around 1.65 mm. The same process was repeated, pictures were taken to see how the flame interacted with the boundary layer and changed as it fell down the tower. With about a 40% decrease in droplet size from before, the same stretching appeared to happen with the 1.65 mm droplets. The flame elongated more and more following the same trend with the 2.35 mm droplets. Again, even smaller droplets were generated to try and prevent boundary layer interaction. This time sub 1 mm droplets were made, a further

83% decrease from 1.65 mm to around .9 mm and tested in the tower. Figure 4.2 shows the evolution of the small droplets near the top, middle, and bottom. They are not the same droplet, but three different ones, which would account for the slight variation between them. However, this shows that the flames stayed a consistent shape falling down the tower. There was a slight variation in flame geometry between the hundreds of images taken at each section, but in general the flames appeared to be near identical. A further decrease in droplet diameter could be done to achieve possibly even better results, however, there was concern with making them too small to the point where they would fully combust before reaching the bottom of the tower or be too small at the bottom making collection and NMR testing impossible.

Figure 4.3 and figure 4.4 are how the flame diameters pictures from the ICMOS camera were quantified. A MATLAB code was made to measure the diameters of the flames by counting the number of pixels and converting that to millimeters. The major axis length is the longer diameter of an ellipse, whereas the minor axis length is the shorter. In this case, the major axis length is the height of the flame from top to bottom, caused by the boundary layer interaction, seen in figure 4.1. This length is seen to increase as the droplets fall for both the 2.35 mm and 1.65, which signified the droplet stretching from the boundary layer interaction, but for the .9 mm droplets, they stayed consistent. Then in figure 4.3, the equivalent diameter is the average of the major and minor axis lengths. For all three sizes, the equivalent diameter stayed constant, with the .9 mm droplets decreasing slightly as the droplet evaporated and burned. To create a spherical droplet, the flow rate of the blower fan was increased or decreased depending on which direction the flame was being pulled. Also, the piezoelectric actuator on the droplet generator can give the smaller droplets an initial

velocity which needed to be taken into account when adjusting the flow rate. With the low Reynolds number, there was no perceived turbulence in the tower, the flames of the droplets did not oscillate or flicker when taking high-speed vides. When using Schlieren imaging the airflow pattern could be seen from the density change caused by the temperature from the hot wire at the top. The heating wire aided in decreasing the viscosity of the air, as well as the hot gas surrounding the flame, and varying the flow rate of the blower fan when adjusting for droplet conditions also helped keep the Reynolds number low. After verifying the consistency in flame diameter and geometry with the small droplets, the change in diameter was then investigated.

n-Octane was used to calculate the change in droplet diameter as it burned. Shadowgraph was used to take pictures of the .9 mm droplets, then another MATLAB code was used to quantify the droplet sizes seen in figure 4.5 and figure 4.6. As the n-Octane combusted down the tower the size of the droplet shrank from around .9 mm down to around .5 mm. There is some variation in the data due to the limitations of the resolution of the high-speed camera and the MATLAB code. Making the distinction on where the droplet started and ended evenly across hundreds of images was a challenge. The diameter change follows a linear fairly linear decrease similar to that shown in the classical d^2 law, but since the droplet flame is not meant to reach extinction, so this graph only shows a section of the change in diameter.

This data and these images reinforce this concept of a forced convection converging channel drop tower. It is able to consistently recreate 1D combustion with spherical flames similar to those in figure 1.1. Sub 1 mm droplets need to be used for this geometry and configuration, but by changing some variables in the design phase it is possible to use larger

droplets, or even droplets in the order of a few hundred microns. These droplets could be collected if the height was decreased to prevent complete combustion.

The way this setup differs from the other methods is in its ability to collect droplets mid combustion. This feature was used to test for preferential vaporization in binary fuel mixtures given in table 3.3 and table 3.4. Both the large droplets and the small droplets were collected and analyzed with NMR to see if there was any change between them. Figure 4.7 and figure 4.8 illustrate the NMR data for n-Heptane before and after combustion. iso-Cetane and the other n-alkanes used are made up of molecules from the paraffinic CH_3 and the paraffinic CH_2 functional groups. The mixtures were 75% by mole fraction iso-Cetane, which is composed primarily of CH_3 functional groups due to it being a branched-chain molecule, where the n-alkanes are made more of more CH_2 functional groups. iso-Cetane has the highest boiling temperature, so it is expected to vaporize and burn off less than the other fuel. Looking at the graphs before and after combustion, the paraffinic CH_2 intensity appears to decrease. n-Heptane is 62.5% paraffinic CH_2. By post processing these NMR graphs, the before and after mole fraction of the mixtures was determined, and figure 4.9 shows the change in mole fraction of the n-alkanes from combusting down the tower. The greater the difference in boiling point between the two fuels, the greater potential for preferential vaporization. n-Heptane has a boiling point more than 140 ^oC lower than iso-Cetane, where n-dodecane is only about 25 ^oC lower There is a slight difference between the change in composition for 2.35 mm droplets and .9 mm droplets. This could be from the interaction of the boundary layer on the burning rate of the fuel, the increase in the size of the flame at the ends of the droplet could cause it to consume more fuel. Or possibly the added convective forces caused a greater evaporation rate.

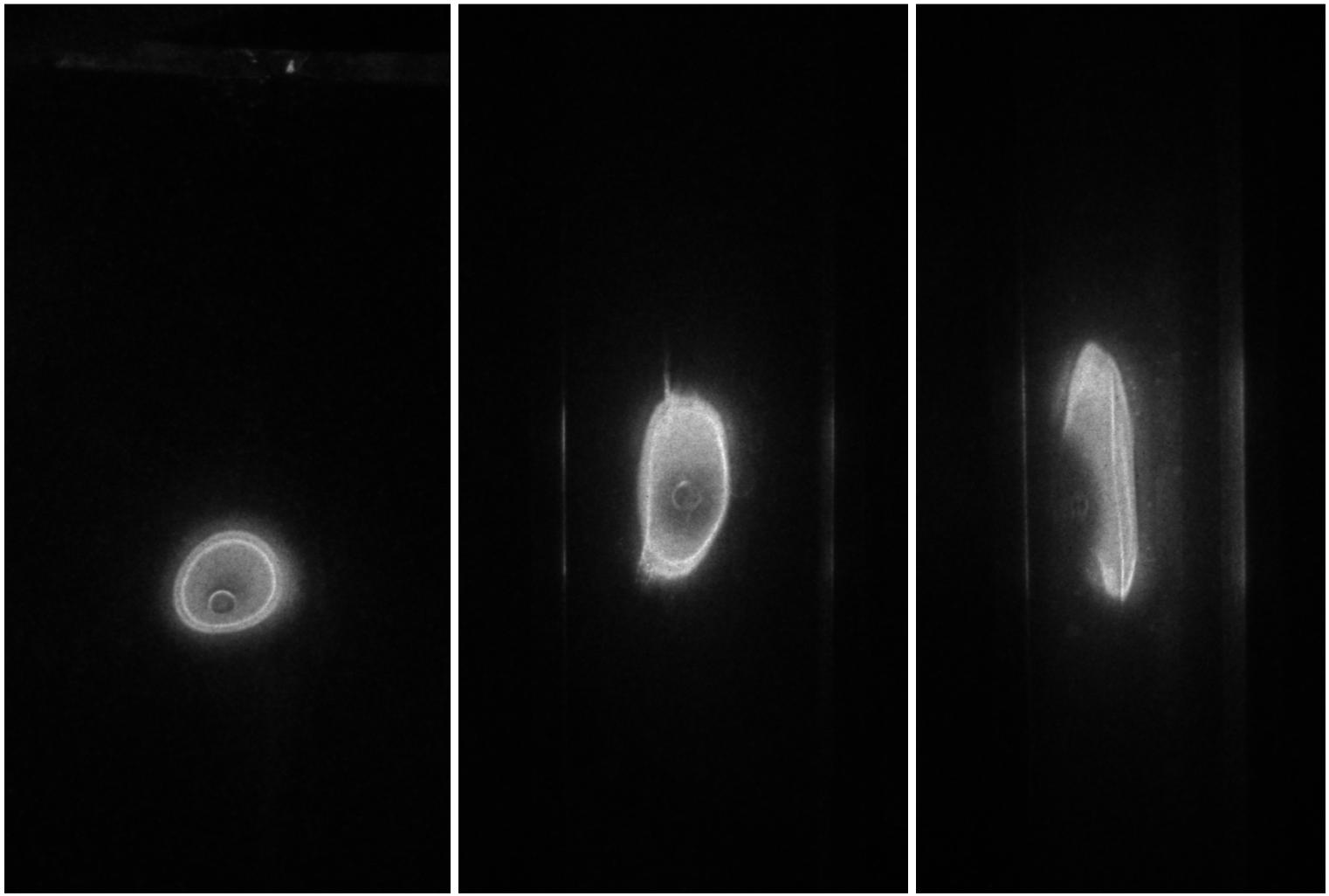

Figure 4.1: 2.35 mm n-Heptane Droplet at 130 mm, 750 mm, and 1420 mm, Using ICMOS Camera

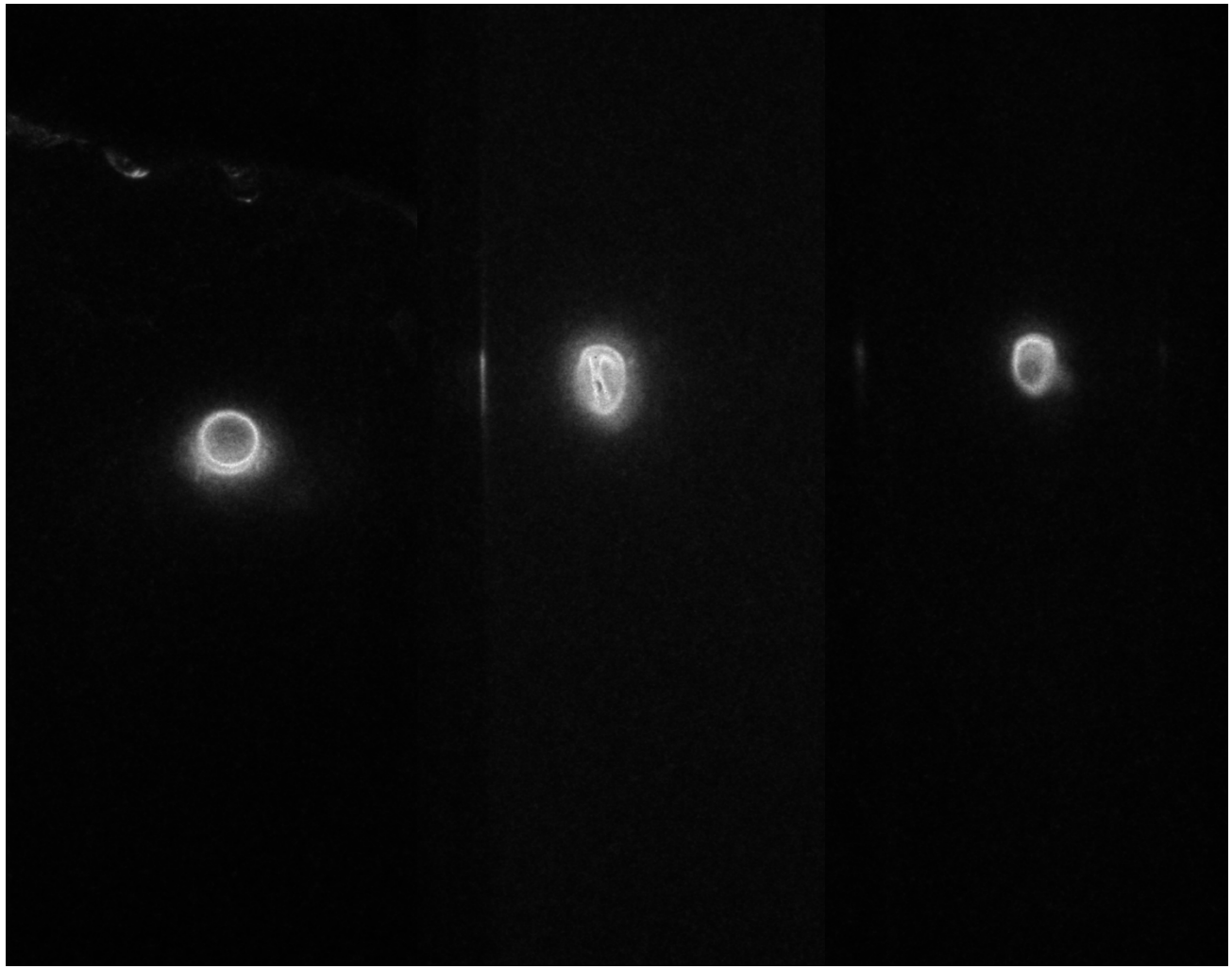

Figure 4.2: .9 mm n-Heptane Droplet at 120 mm, 805 mm, and 1445 mm, Using ICMOS Camera

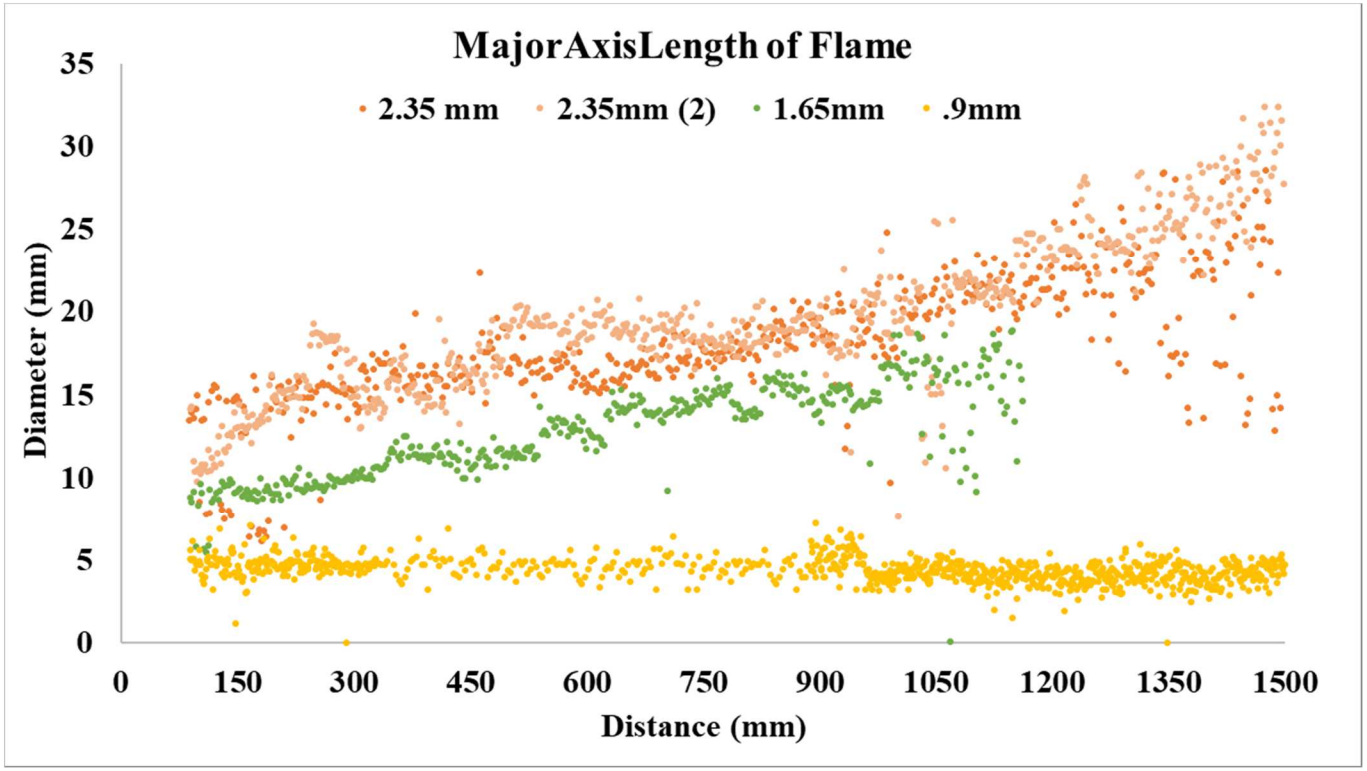

Figure 4.3: Major Axis Length of Droplet Flames

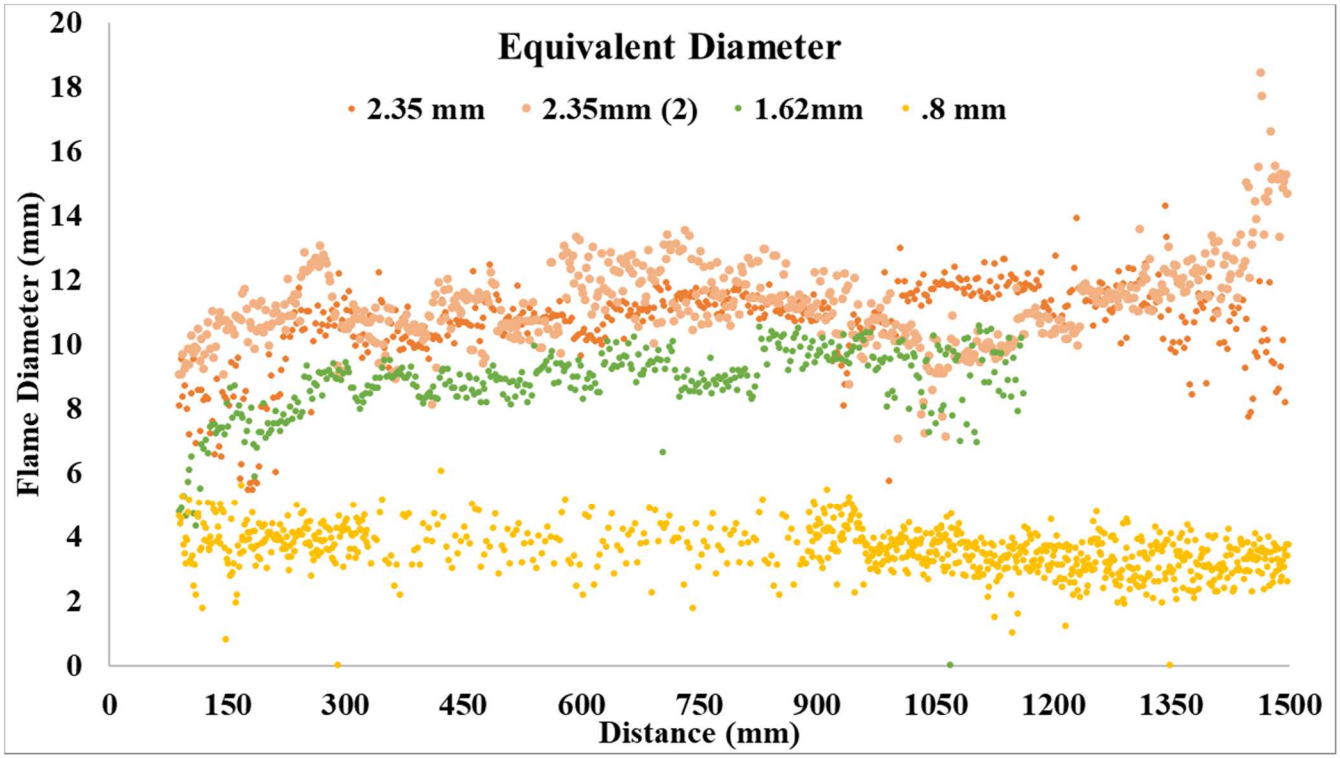

Figure 4.4: Equivalent Diameter of Droplet Flames

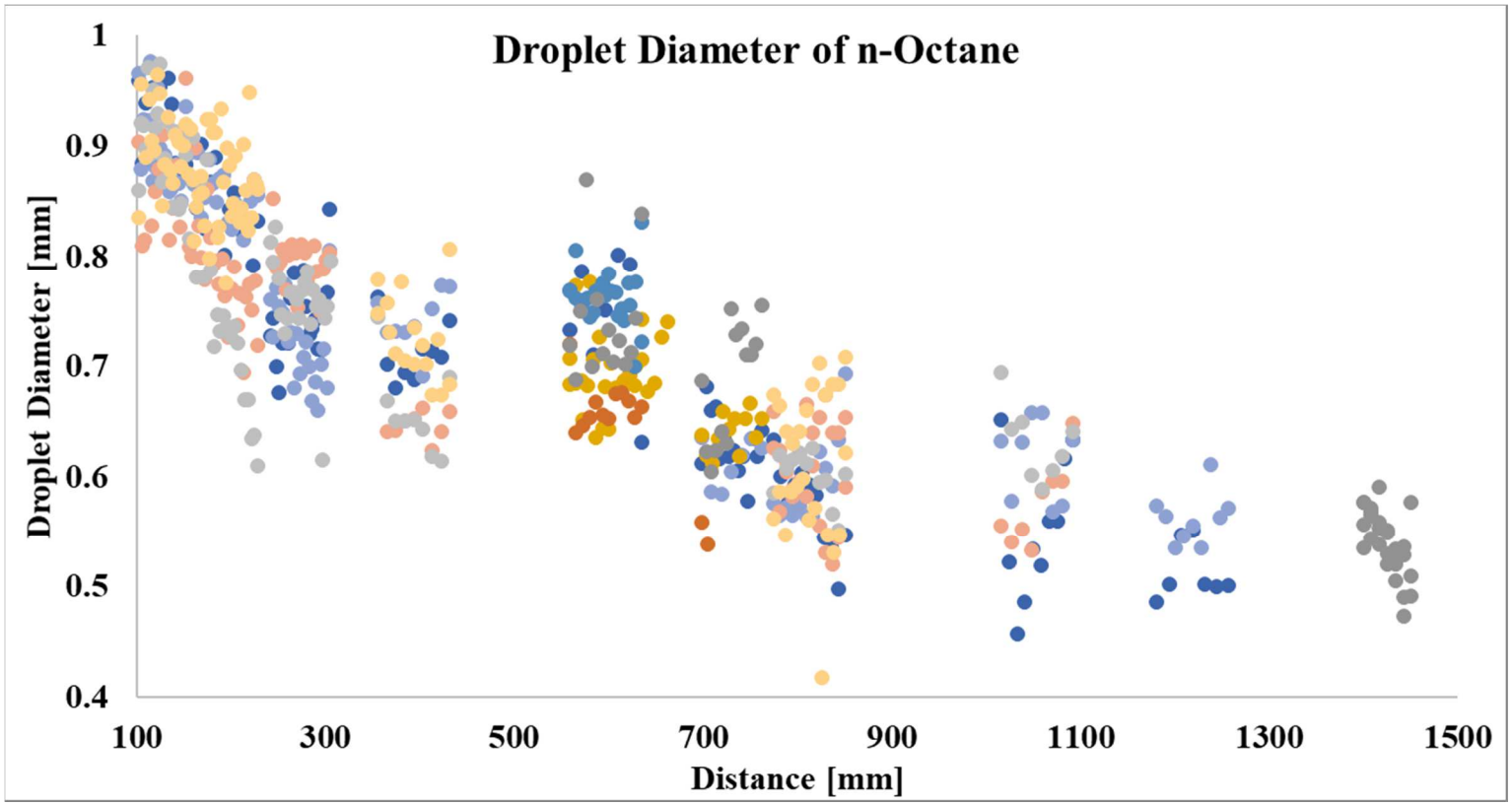

Figure 4.5: Droplet Diameters of n-Octane

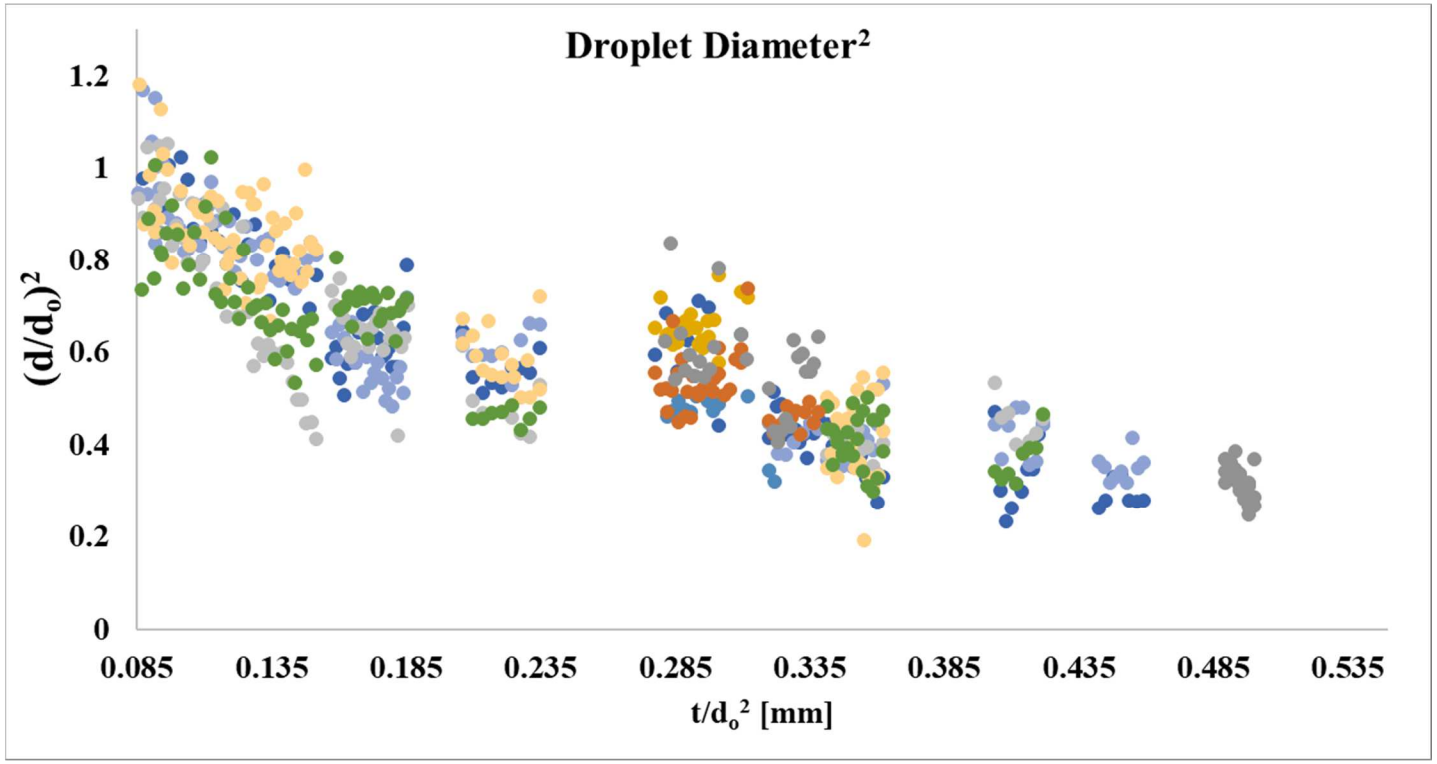

Figure 4.6: Droplet Diameters of n-Octane with d^2 law Droplet Diameters of n-Octane

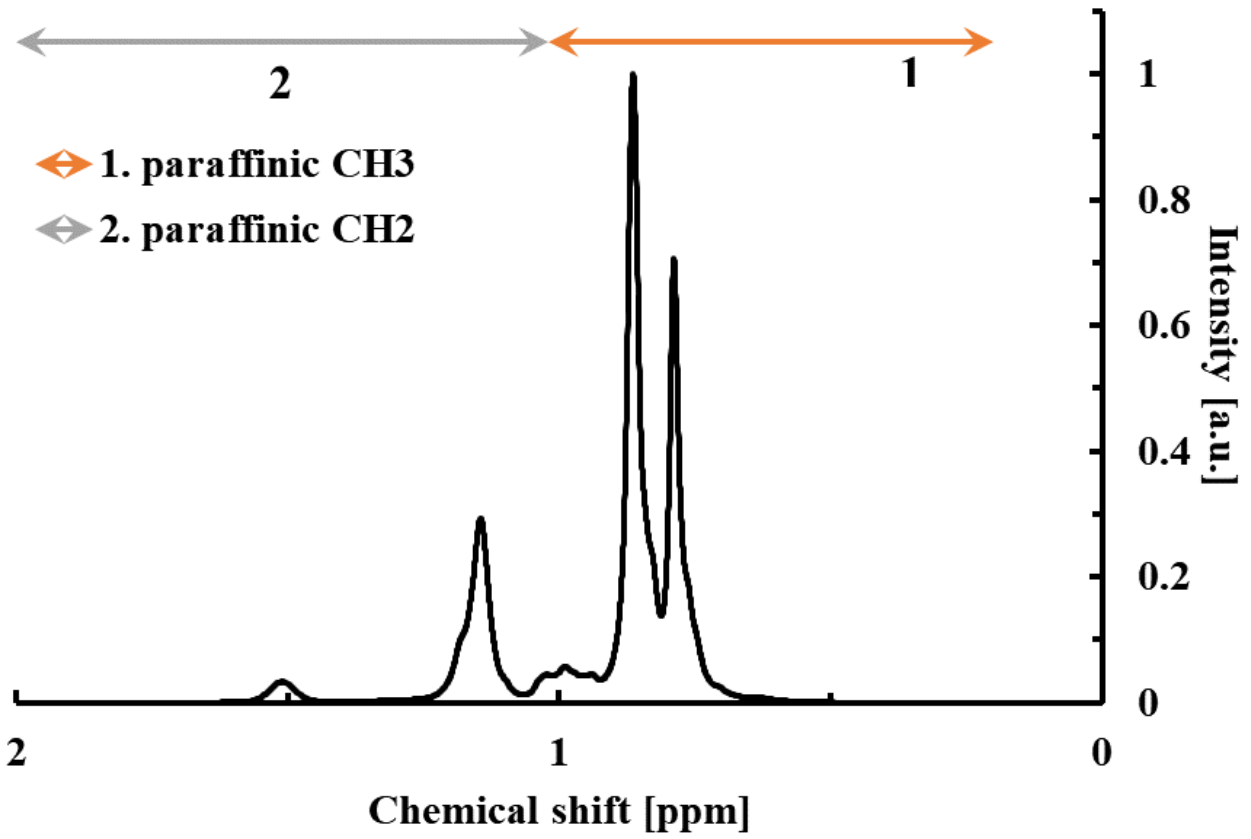

Figure 4.7: NMR of 75/25 iso-Cetane/n-Heptane Before Combustion

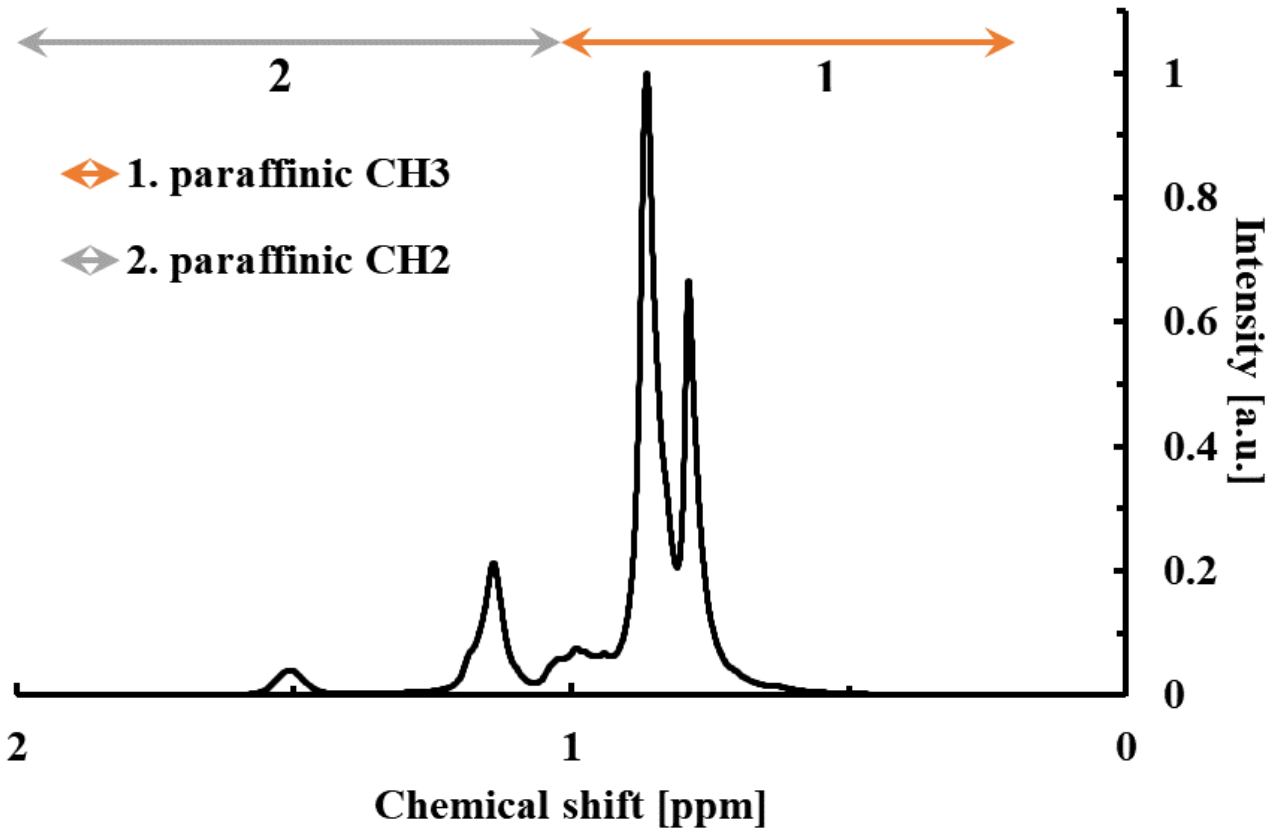

Figure 4.8: NMR of 75/25 iso-Cetane/n-Heptane After Combustion

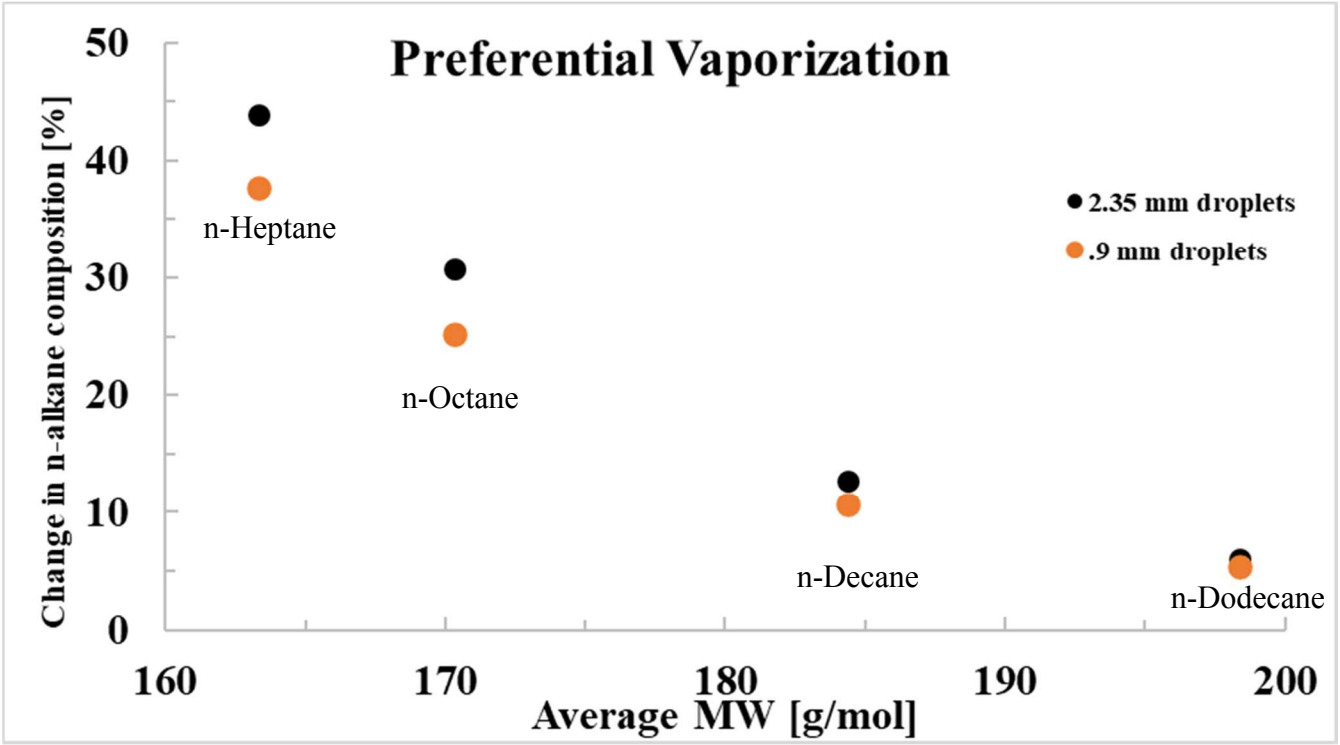

Figure 4.9: Preferential Vaporization Potential

CHAPTER 5

CONCLUSION

The goal of this research is to create and validate an alternate method of the recreation of microgravity combustion that is cheaper and more accessible than the options available along with achieving near the same results as said methods. The design, fabrication, and testing of a converging-channel drop tower for sphere symmetric isolated single droplet combustion using forced convection was done to simulate microgravity combustion. A droplet generator was made to control drop size to prevent boundary layer interaction that would stretch the flame. A High speed and ICMOS camera were used to capture images of the droplets and their flames down the length of the tower to validate 1D combustion. These pictures were processed to see how the droplets changed in size and see if the flames remained spherical.

Many images were taken and analyzed the diameter change was found for n-Octane to see if it followed the d^2 law, but the residence time of the drop tower wasn't long enough to see any noticeable change for the size of droplets used. Changing the droplet diameter to under 1mm helped solve the issue of boundary layer interaction on the flame, and the flame was able to stay at a constant diameter as it fell.

Since the samples could be collected mid combustion, binary mixtures were used to see the impact of preferential vaporization in a 1D environment using NMR. Iso-Cetane was mixed with n-alkanes of increasing molecular weight, then tested in the tower and collected at the bottom. The n-Heptane mixture showed the most preferential

vaporization potential due to it having the greatest difference in boiling point, where n-Dodecane had the least. It is to be expected that fuels with similar boiling points will combust more proportionally than those without.

The far future of combustion research is unknown, with dwindling oil and gas reserves, the increase in emission standards, electric vehicles, and a pledge to be carbon neutral by 2050 from the UN, oil might soon be phased out for cleaner, renewable energy sources. In the meantime, hydrocarbon fuels have a strong presence in the world which facilitates a need to research, improve, and innovate to make a better tomorrow, today.

REFERENCES

(1) *"Sputnik and the Dawn of the Space Age." Edited by Garrett Shea, NASA History Division, NASA.*

(2) *Gokoglu, Suleyman A., et al. A Researcher's Guide to ISS Combustion Science - NASA. Edited by Amelia Rai, 2015.*

(3) *Kono, Michikata, et al. "Current State of Combustion Research in Microgravity." Symposium (International) on Combustion, vol. 26, no. 1, 1996, pp. 1189–1199., https://doi.org/10.1016/s0082-0784(96)80335-3.*

(4) *Dunbar, Brian. "What Is Microgravity?" NASA, NASA, 16 June 2015, https://www.nasa.gov/audience/forstudents/5-8/features/nasa-knows/what-is-microgravity-58.html.*

(5) *"Scientific Research Services." AirZeroG, https://www.airzerog.com/scientific-research-services/.*

(6) *Pletser, Vladimir. "European Aircraft Parabolic Flights for Microgravity Research, Applications and Exploration: A Review." REACH, vol. 1, 2016, pp. 11–19., https://doi.org/10.1016/j.reach.2016.05.002.*

(7) *"2.2 Second Drop Tower - Glenn Research Center." NASA, NASA, 21 Jan. 2020, https://www1.grc.nasa.gov/facilities/drop/.*

(8) *Zhang, Xiaoqian, et al. "Some Key Technics of Drop Tower Experiment Device of National Microgravity Laboratory (China) (NMLC)." Science China Technological Sciences, Science in China Press, 29 Dec. 2004, https://link.springer.com/article/10.1360%2F102004-21.*

(9) *Sun, Peiyi, et al. "Microgravity Combustion of Polyethylene Droplet in Drop Tower." Combustion and Flame, vol. 222, 2020, pp. 18–26., https://doi.org/10.1016/j.combustflame.2020.08.032.*

(10) *Liu, T. Y., et al. "Microgravity Level Measurement of the Beijing Drop Tower Using a Sensitive Accelerometer." Scientific Reports, vol. 6, no. 1, 2016, https://doi.org/10.1038/srep31632.*

(11) *Kono, Michikata, et al. "Current State of Combustion Research in Microgravity." Symposium (International) on Combustion, vol. 26, no. 1, 1996, pp. 1189–1199., https://doi.org/10.1016/s0082-0784(96)80335-3.*

(12) *Boen, Brooke. "Microgravity Research Program Fact Sheet (01/99)." NASA, NASA, 1998, https://www.nasa.gov/centers/marshall/news/background/facts/microgravity.html#backtoTop.*

(13) *Wild, Flint. "What Is the International Space Station?" NASA, NASA, 2 June 2015, https://www.nasa.gov/audience/forstudents/5-8/features/nasa-knows/what-is-the-iss-58.html.*

(14) *"U.S. Energy Information Administration - EIA - Independent Statistics and Analysis." Renewable Energy Explained - U.S. Energy Information Administration (EIA), 2020, https://www.eia.gov/energyexplained/renewable-sources/.*

(15) *Adams, Sean Patrick. "The US Coal Industry in the Nineteenth Century." EHnet, https://eh.net/encyclopedia/the-us-coal-industry-in-the-nineteenth-century-2/.*

(16) *I. Hore-Lacy, "Future Energy Demand and Supply," in Nuclear Energy in the 21st Century, 2nd ed., London, UK: WNUP, 2011, ch.1, sec.6, pp.9*

(17) *History.com Editors. "Oil Industry." History.com, A&E Television Networks, 8 Apr. 2010, https://www.history.com/topics/industrial-revolution/oil-industry.*

(18) *"History of Reducing Air Pollution from Transportation in the United States." EPA, Environmental Protection Agency, 2021, https://www.epa.gov/transportation-air-pollution-and-climate-change/accomplishments-and-success-air-pollution-transportation.*

(19) *Guterres, António. "Carbon Neutrality by 2050: The World's Most Urgent Mission Secretary-General." United Nations, United Nations, 11 Dec. 2020, https://www.un.org/sg/en/content/sg/articles/2020-12-11/carbon-neutrality-2050-the-world%E2%80%99s-most-urgent-mission.*

(20) *V. Nayagam1 , D. Dietrich2 , P. Ferkul1 , M. C. Hicks2 and F. A. Williams3. Methanol Droplet Extinction in Oxygen/Carbon-Dioxide/Nitrogen Mixtures in Microgravity: Results from the International Space Station Experiments. 9 Oct. 2012, https://www1.grc.nasa.gov/wp-content/uploads/Nayagam_ESSCI_2011.pdf.*

(21) *Hawersaat, Robert. "Slice - Glenn Research Center." NASA, NASA, 25 Nov. 2019, https://www1.grc.nasa.gov/space/iss-research/msg/slice/.*

(22) *Farouk, Tanvir I., et al. "Sub-Millimeter Sized Multi-Component Jet Fuel Surrogate Droplet Combustion: Physicochemical Preferential Vaporization Effects." Proceedings of the Combustion Institute, vol. 38, no. 2, 2021, pp. 3313–3323., https://doi.org/10.1016/j.proci.2020.06.200.*

(23) *D. F. Wang, J. S. Woo, and B. D. Shaw, "A drop□tube apparatus to promote spherically symmetric evaporation and combustion of unsupported droplets", Review of Scientific Instruments 62, 3029-3036 (1991)*

(24) *Choi, Mun Young. "Droplet Combustion Characteristics Under Microgravity and Normal-Gravity Conditions." Order No. 9230621 Princeton University, 1992. Ann Arbor: ProQuest. Web. 13 Nov. 2021.*

(25) *Won, Sang Hee, et al. "Preferential Vaporization Impacts on Lean Blow-out of Liquid Fueled Combustors." Combustion and Flame, vol. 205, 2019, pp. 295–304., https://doi.org/10.1016/j.combustflame.2019.04.008.*

(26) *Bell, David C., et al. "The Impact of Preferential Vaporization on Lean Blowout in a Referee Combustor at Figure of Merit Conditions." Volume 1: Fuels, Combustion, and Material Handling; Combustion Turbines Combined Cycles; Boilers and Heat Recovery Steam Generators; Virtual Plant and Cyber-Physical Systems; Plant Development and Construction; Renewable Energy Systems, 2018, https://doi.org/10.1115/power2018-7432.*

(27) *Farouk, Tanvir I., et al. "Sub-Millimeter Sized Multi-Component Jet Fuel Surrogate Droplet Combustion: Physicochemical Preferential Vaporization Effects." Proceedings of the Combustion Institute, vol. 38, no. 2, 2021, pp. 3313–3323., https://doi.org/10.1016/j.proci.2020.06.200.*